Journal of Industrial and Management Optimization

JIMO, 22(1): 642–690.
DOI: 10.3934/jimo.2026024
Received: 09 September 2025
Revised: 11 November 2025
Accepted: 21 November 2025
Published: 18 December 2025

https://www.aimspress.com/journal/jimo

Research article

A Modified Lyrebird Optimization for Single, Double, and Triple Diode Parameters PV Cell Extraction

Sultan Hakmi[1], Hashim Alnami[1], Ghareeb Moustafa[1], Badr M Al Faiya[1] and Ahmed Ginidi[2,*]

[1] Department of Electrical and Electronics Engineering, Faculty of Engineering and Computer Science, Jazan University, Jizan 45142, Saudi Arabia
[2] Department of Electrical Engineering, Faculty of Engineering, Suez University, P.O. Box: 43221, Suez, Egypt

* **Correspondence:** Email: ahmed.ginidi@eng.suezuni.edu.eg.

Abstract: Accurate modeling of photovoltaic (PV) cells is essential for performance assessment, control, and optimization of solar energy systems. The diode circuit models, particularly the single-diode (SD), double-diode (DD), and triple-diode (TD) structures, are widely adopted for characterizing PV behavior; however, extracting their unknown parameters is a challenging nonlinear, multimodal optimization problem. To address these challenges, this study proposes a modified lyrebird optimization (MLO) algorithm, an enhanced variant of the recently developed LO. It integrates a memory-based learn search strategy (MBLSS) to reinforce exploration and a diversity maintenance learn search strategy (DMLSS) to refine exploitation. The algorithm was employed to extract parameters of both the RTC France solar cell and the Solarex MSX-60 PV module under SD, DD, and TD models. Extensive simulations and statistical analyses demonstrated that the proposed MLO significantly outperforms the conventional LO and a wide range of metaheuristic and analytical methods in terms of root mean square error (RMSE), convergence speed, stability, and robustness across multiple runs. In the MSX-60 module tests, the proposed MLO reduced the RMSE by more than 55% compared to the conventional LO and achieved a stable mean RMSE of 1.75×10^{-3} over 50 independent runs. Similarly, for the RTC France solar cell, MLO achieved a minimum RMSE of 9.82×10^{-4}, outperforming several recently reported metaheuristics. Moreover, the proposed MLO was extended and validated on the Shell S75 monocrystalline module under different irradiance and temperature conditions. The results demonstrated consistently lower RMSE values and near-zero variance across operating ranges, confirming the robustness and stability of MLO in practical PV environments. The strong agreement between simulated and experimental I–V and P–V characteristics

confirms the reliability of the extracted parameters. These findings highlight the potential of MLO as a robust and accurate tool for PV modeling, with promising applications in solar system design, performance evaluation, and predictive energy management.

Keywords: Lyrebird optimization; Modified lyrebird optimization; Parameters PV cell extraction; Single diode; Double diode; Triple diode model
Mathematics Subject Classification: Primary: 90B99; Secondary: 90C59

1. Introduction

Solar PV energy has emerged as a crucial part of contemporary energy systems as the world's energy transition quickens and the need for sustainable energy sources keeps rising [1]. Solar PV, being clean and renewable, has become a vital technology for lowering greenhouse gas emissions and attaining energy independence. Accurate PV power generation modeling is necessary to realize the entire potential of solar PV [2]. These models serve as the basis for efficient system approach performance analysis, fault detection, and energy forecasting by enabling accurate simulation, evaluation, control, and optimization of PV systems. Furthermore, optimizing energy distribution across power grids, strengthening energy management tactics, and increasing energy efficiency all depend on accurate models [3]. The diode circuit model, which has a strong physical foundation and allows for accurate characterization of the current–voltage (I–V) behavior of solar cells under a variety of environmental conditions, stands out among the other modeling approaches [4].

The SD [4] and DD [5] models are two categories into which the diode circuit model can be divided based on the necessary level of complexity and accuracy. Five or seven unknown parameters in the two models need to be obtained for the simulation. Furthermore, obtaining these parameters is extremely difficult because PV models are nonlinear, multi-variable, and multimodal. Thus, a major area of research continues to be the development of effective and precise techniques for obtaining PV model parameters.

The diode circuit model, which may be divided into two primary categories, is the primary focus of the parameter extraction techniques that are currently being studied. The analytical method represents the first category of parameter identification approaches. It makes use of key data points, including the maximum power point, open-circuit voltage, and short-circuit current, to solve equations and determine model parameters. This technique involves addressing a series of transcendental equations at critical points of the I–V characteristic curve, and it has been widely applied for extracting PV model parameters [6]. The primary benefits are a quicker computation, a more straightforward method, a reduction in calculation time, and accurate results. In [7], a quick and precise analytical method was proposed using datasheets made accessible by the manufacturers. Later, an approach based on Lambert's W-function—a precise and impromptu analytical technique—was proposed in [8]. Additionally, in [9], a different analysis technique based on the Co-content function was proposed. In recent years, a graphical technique has been used to solve analytical problems [10]. The approach has significant disadvantages but requires the least quantity of data. Due to its enormous complexity, the set of equations is challenging to solve, and the solution process is prone to divergence. Additionally, the chosen data points have a significant impact on the model's correctness, and errors in these points reduce the overall reliability of the model.

The optimization method, which has drawn more attention recently [11], is the second category. The category, which may be further separated into deterministic and metaheuristic approaches, makes use of measured data, such as I–V curve data, and uses numerical optimization techniques to reduce the error between simulated and measured current data. Initial values and mathematical models are essential to the deterministic approach. Therefore, the computation tends to deviate if the mathematical model is intricate or if the starting values are poorly established. Conversely, the metaheuristic approach could successfully circumvent the aforementioned problem. It is extensively useful in engineering optimization since it is straightforward, effective, and independent of intricate mathematical models or initial values.

In terms of calculating the parameters as efficiently as possible, numerical procedures are more accurate than analytical methods. This is because every point on the characteristic curve is taken into account throughout the study. In order to estimate the five parameters of a PV cell, numerical methods based on Newton's method and nonlinear least squares were first proposed in [12]. A resistive-companion approach was then suggested in [13], and it produced findings that were somewhat superior to the analytical ones. Later on, it was proposed to use Newton–Raphson-based improvisation to determine parameters for solar PV modules [14]. The prolonged computation time is the main drawback of all numerical-based methods. In addition to the aforementioned issues, these methods may result in less accurate findings, especially when it comes to recognizing a lot of solar PV factors and only providing approximate initial circumstances. These methods also rely on the circumstances of the previous system, and there is a greater chance that the solution will be trapped at local minima.

In [15], a JAYA variant driven by individual weights (DIWJAYA) was introduced for PV parameters extraction. This improved version was based on changing the individuals by going toward the best candidate and away from the worst, using a weight factor for every individual. This change helped people stay away from bad options early on in their search course while carefully getting closer to the best one overall. Additionally, a Gaussian mutation process was incorporated to support solutions' quality and diversity by introducing regulated perturbations. In [16], an improved version of the butterfly optimizer (BFO) incorporating a chaos learning strategy (CLS) was presented to support the BFO's slow convergence and reduce its susceptibility to local optima. The integrated CLS employed chaotic maps, using tent and logistic shapes, to generate pseudorandom numbers. This enhanced BFO variation integrated a Cauchy mutation to provide extensive variations in the population and an effective elimination system for substituting underperforming individuals, hence expediting convergence. It was successfully evaluated on CEC 2022 benchmark functions, and its applications were extended for PV parameter estimation on a real YL PV power station in Guizhou, China. In [17], a hybrid optimization approach combining the differential evolution algorithm (DEA) and the backtracking search technique (BST) was performed to extract PV parameters under varied environmental conditions. This hybrid method started the population inside the limits of the parameters and used BST's tuned adjustments to mix the existing and new populations. It also used DEA's mutation operators following BST's preliminary selection, which gave a range of options that DEA improved for better convergence. A kangaroo escape optimizer (KEO) was introduced in [18] to discover PV parameters that depict zigzag maneuvers, long jumping, decoy throwing, and exploring safer locations. This approach was motivated by the predator escape behaviors of kangaroos and was used for PV estimate on benchmarks such as Photowatt-PWP201 and RTC France. In this KEO approach, to avoid stagnation, dimensions were probabilistically hidden during updates via a decoy drop technique. Also, a chaotic logistic mapping was used to describe energy levels and flexible transfer strategies for

reduced energy shifts to big leaps for variety, while high energy favors zigzag escaping. In [19], an integrated analytical Newton–Raphson-based optimizer (NRBO) was developed, with the analytical technique generating starting parameter predictions from important I–V points, minimizing reliance on random beginnings. In order to reduce the RMSE for the RTC France and solar power panels, NRBO then improved these using NRBO's phases. To determine the PV attributes in the current circumstance, parameter estimation methods based on various metaheuristics were established and put into practice, such as orthogonally-adapted gradient-based optimization (OLGBO) [20], artificial rabbits algorithm [21], improved grey wolf optimizer (IGWO) [22], symmetric chaotic gradient-based optimizer (SC-GBO) [23], enhanced vibrating particles system (EVPS) [24], tree growth algorithm (TGA) [25], social network search algorithm [26], chaotic-driven tuna swarm optimizer (CTSO) [27], arithmetic optimization algorithm (AOA) [28], enhanced prairie dog optimizer (EnPDO) [29], hybrid successive discretization algorithm (HSDA) [30], heap-based algorithm [31], general algebraic modeling system (GAMS) [32], mountain gazelle optimizer (MGO) [33], and marine predator algorithm (MPA) [34].

In [35], the Harris hawks optimizer (HHO) was enhanced by incorporating a chaotic drift mechanism along with an adversarial-based exploratory strategy. Similarly, [36] introduced an improved ant–lion optimizer (IALO) for parameter estimation, which demonstrated promising results. To achieve a more stable and efficient model and to accurately characterize PV system behavior, an augmented mutation Harris hawks optimizer (AMHHO) was proposed in [37], enabling faster convergence and precise assessment of solar cell simulation parameters. In [38], an enhanced sine cosine (ESC) algorithm was presented to estimate unknown parameters in both single-diode (SD) and double-diode (DD) PV models. Furthermore, [39] reported the application of an upgraded Harris hawks optimizer (CCNMHHO) for PV parameter extraction. To improve global convergence and local exploitation capabilities, the moth-flame optimization (MFO) method was employed in [40] for identifying PV module parameters, yielding excellent performance in SD and DD model configurations. In [41], an improved PSO was illustrated by using quadratic interpolation to accelerate convergence and a local search strategy to avoid stagnation in local minima to determine the unknown parameters of SD and DD. By integrating drone squadron optimization with the Newton–Raphson performance technique, the exact constituent PV module parameters were retrieved in [42]. Another study [43] improved the population diversity and exploration operator of the moth-flame algorithm by using local escape operators. Although this algorithm required a lot of function evaluations, it could yield very good results when compared to other approaches. In [44], a squirrel search algorithm was adjusted by minimizing the RMSE in order to estimate the unknown parameters of SD and DD models.

These methods are suggested to address the inherent drawbacks of each method, allow for various combinations of individual methods, and then show up as a capable method to determine the parameters of solar PV models. However, the effectiveness of these methods varies depending on the situation. Also, the careful choice of algorithm control parameters governs their accuracy, robustness, and rate of convergence. In this work, an improved metaheuristic approach with adaptively altering control parameters is selected among these two options.

The current work is driven by these research gaps to develop a more effective method for identifying and testing solar PV parameters in a wide range of scenarios, which is ideal for real-time applications. The effectiveness of searching throughout the exploitation and exploration stages is significantly increased by adaptively modifying the control parameters, both in the case of LO and other stochastic techniques. MLO integrates a memory-based learn search strategy (MBLSS) to reinforce exploration and a diversity maintenance learn search strategy (DMLSS) to refine exploitation.

These two strategies can achieve better accuracy with faster convergence, leading to optimal parameter values, increasing overall performance, and avoiding confinement problems at local minima. The main contributions are:

- To determine the parameters of different PV cells and modules, a modified approach known as MLO is described.
- A number of simulation examples and statistical findings are shown and examined in order to evaluate the effectiveness of the suggested MLO method.
- MLO achieves the best overall performance, obtaining the lowest average rank (1.40) among twelve algorithms in the Friedman analysis.
- Post-hoc and Wilcoxon tests confirm that the performance improvements of MLO over LO and most benchmark algorithms are statistically significant ($p < 0.05$), demonstrating both higher accuracy and repeatability.
- When applied to PV cell parameter extraction, MLO consistently yields lower RMSE and more stable convergence, confirming its effectiveness for practical photovoltaic model identification.
- The proposed MLO is further validated on the Shell S75 PV module under varying irradiance (200–1000 W/m²) and temperature (25–60 °C) conditions, where it consistently outperforms the original LO and maintains extremely low standard deviation ($\approx 10^{-17}$–10^{-18}), confirming its robustness and strong generalization capability across real operating scenario variations.

The article's general format is as follows: In addition to outlining the study's contribution, Section 1 provides the background and motivation. After a brief introduction, Section 2 provides a thorough explanation of solar PV modeling and the objective formulation, while taking into account all relevant restrictions and system factors. A description of the suggested LO and MLO techniques is specified in Section 3, together with a list of all the significant changes that have been suggested and the statistical results. Section 4 presents an analysis and illustration of the identification and simulation results, while Section 5 offers the conclusion of this work.

2. Problem formulation of solar PV parameters extraction

It is necessary to propose a number of simplified and intricate models in order to ensure correct design, simulation, and analysis. In this section, various PV models are briefly described together with their corresponding parameters and the formulation of their goal functions.

2.1. PV cell model based on SD

An antiparallel diode, a series resistor, a shunt resistor, and a photon-generated current source make up the PV cell model's SD-based electrical equivalent circuit. The aforementioned paradigm is illustrated in Figure 1 [45]. Applying Kirchhoff's current law (KCL) to Figure 1 yields the following equation.

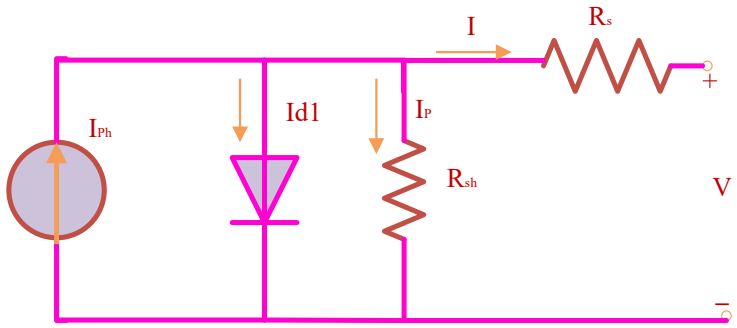

Figure 1. SD model representation.

$$I_{ph} = I_P + I_{d1} + I \tag{1}$$

where I_{ph}, I_{d1}, and I_P stand for photon-generated current, diode current, and shunt resistance R_p current, respectively. Furthermore, I, V, and R_s stand for the PV cell voltage, current, and series resistance, respectively. The expression for the current flowing through R_p is:

$$I_P = \frac{I \cdot R_S + V}{R_{Sh}} \tag{2}$$

$$I_{d1} = I_{S1}\left[\exp\left(\frac{I \cdot R_S + V}{\eta_1 \cdot V_t}\right) - 1\right] \tag{3}$$

where I, η_1, and V_{thr} stand for the diode's saturation current, ideality factor, and thermal voltage, respectively. The following is an expression of the current relationship:

$$V_{thr} = \frac{K_B \cdot T}{q} \tag{4}$$

where T, q, and K_B represent temperature in K for the cell/module, the Boltzmann constant (1.38065×10^{-23}) in J/K, and the electron charge (1.60217×10^{-19}) in C, respectively. Eq. (5) is used to determine the PV cell current using Eqs. (1), (2), and (3) as follows:

$$I = I_{ph} - I_{S1}\left[\exp\left(\frac{I \cdot R_S + V}{\eta_1 \cdot V_{thr}}\right) - 1\right] - \frac{V}{R_{sh}} - I.\frac{R_S}{R_{sh}} \tag{5}$$

2.2. PV cell model based on DD

Two diodes antiparallel to the current source, a photon-generated source of current, a series resistor, and a shunt resistor make up the electric equivalent circuit of a PV cell model based on double

diodes. The DD model is illustrated in Figure 2. When KCL is applied to Figure 2, the following equation is produced:

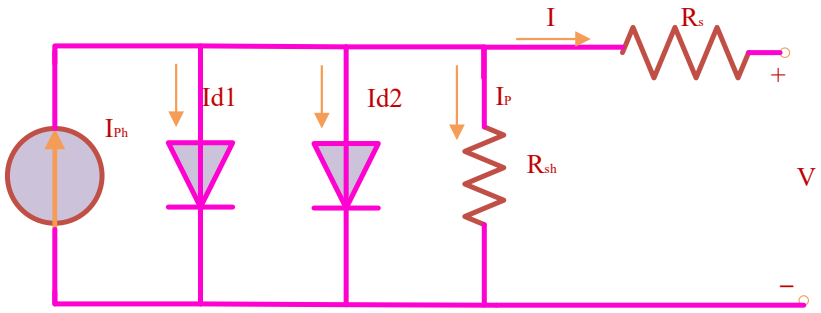

Figure 2. DD model representation.

$$I_{ph} = I + I_{Sh} + I_{d1} + I_{d2} \tag{6}$$

where I_{d1} and I_{d2} indicate the current flowing in diodes *D1* and D2, while I_{Sh} and I indicate the current through the shunt resistance R_p and cell output current, respectively. Moreover, I_{ph} represents the photon-produced current.

The current passing in diode D2 could be written as follows in Eq. (7):

$$I_{d2} = I_{S2}\left[\exp\left(\frac{I \cdot R_S + V}{\eta_2 \cdot V_t}\right) - 1\right] \tag{7}$$

where η_2 represents diode *D2*'s ideality factor, and I_{S2} represents its saturation current. Consequently, the PV cell output current is provided as follows:

$$I = I_{ph} - I_{S1}\left[\exp\left(\frac{I \cdot R_S + V}{\eta_1 \cdot V_{thr}}\right) - 1\right] - I_{S2}\left[\exp\left(\frac{I \cdot R_S + V}{\eta_2 \cdot V_{thr}}\right) - 1\right] - \frac{V}{R_{sh}} - \frac{I \cdot R_S}{R_{sh}} \tag{8}$$

2.3. PV cell model based on TD

In addition to the components in the DD model, an additional antiparallel diode is added to make up the triple diode equivalent electric circuit, as shown in Figure 3 [22, 25,46]. The following equation is obtained by applying KCL to Figure 3.

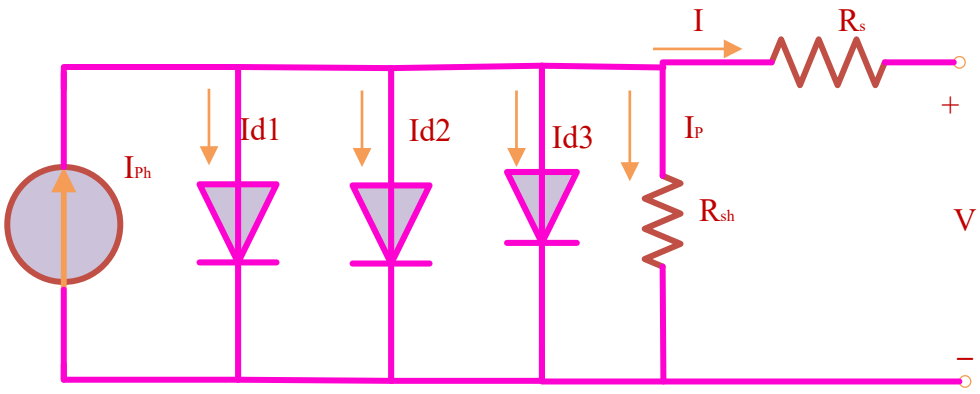

Figure 3. TD model representation.

$$I_{ph} = I + I_{Sh} + I_{d1} + I_{d2} + I_{d3} \tag{9}$$

where I_{d3} indicates the current flowing in diode D3.

The current in diode D3 can be written as follows in Eq. (10):

$$I_{d3} = I_{S3}\left[\exp\left(\frac{I \cdot R_S + V}{\eta_3 \cdot V_t}\right) - 1\right] \tag{10}$$

where η_3 represents diode *D2*'s ideality factor, and I_{S3} represents its saturation current. Consequently, the PV cell output current is provided as follows:

$$\begin{aligned} I = I_{ph} - \frac{V}{R_{sh}} - \frac{I \cdot R_S}{R_{sh}} - I_{S1}\left[\exp\left(\frac{I \cdot R_S + V}{\eta_1 \cdot V_{thr}}\right) - 1\right] \\ - I_{S2}\left[\exp\left(\frac{I \cdot R_S + V}{\eta_2 \cdot V_{thr}}\right) - 1\right] - I_{S3}\left[\exp\left(\frac{I \cdot R_S + V}{\eta_3 \cdot V_{thr}}\right) - 1\right] \end{aligned} \tag{11}$$

2.4. Model of PV modules

PV modules are made up of solar cells linked in series or series-parallel configurations. The PV modules used in this investigation are made up of N_S and N_P solar cell series and parallel combinations. Eq. (12) provides the PV module's output current if it consists of a SD-based PV cell [47].

$$\begin{aligned} I = N_p\left(I_{ph} - I_{S1}\left[\exp\left(\frac{1}{\eta_1 \cdot N_s \cdot V_t} \times \left(\frac{V}{N_p} + \frac{I \cdot N_s \cdot R_S}{N_p}\right)\right) - 1\right]\right) \\ - \frac{1}{N_s \cdot N_p \cdot R_{sh}} \times \left(\frac{V}{N_p} + \frac{I \cdot N_s \cdot R_S}{N_p}\right) \end{aligned} \tag{12}$$

2.5. Formulation of the objective function

The task of identifying parameters for the PV model is converted into a single-objective optimization problem [48]. The RMSE between the predicted (estimated) and experimental currents of the PV models under discussion is used as the sole objective function (OF) for this work. Consequently, the following formulation of the optimization problem [49] is illustrated:

$$RMSE = \sqrt{\frac{1}{PM}\left(\sum_{K=1}^{PM}(I_{cal}^{K}(V_{exp}^{K}, y) - I_{exp}^{K})^2\right)} \tag{13}$$

where PM represents the number of experimental I–V data points of the PV model being examined, k represents the experimental data index, y signifies the set of parameters of the PV model that has to be found, and $I_{cal}^{K}(V_{exp}^{K}, y)$ represents the PV model's current error function [50]. A better y is found if the RMSE value is very tiny. In order to achieve ideal settings, the goal is to use MLO to minimize RMSE.

3. Proposed MLO approach for PV parameter estimation

The LO algorithm, which focuses on the lyrebird's inherent ability to recognize and respond to external dangers, is based on the lyrebird's natural threat-response behaviors [51]. It moves through the area and decides whether to blend in or flee to a safer spot when it senses a potential threat [52]. The adaptive behavior of the LO algorithm allows it to navigate difficult optimization contexts.

3.1. Initialization of bird's locations

The first step in the LO algorithmic process is to randomly initialize the bird placements inside the designated borders while taking into account each bird's size (*NBs*). Within this framework, a lyrebird corresponds to a candidate solution expressed as a position vector (*LB*) in a *d*-dimensional search space. As shown in equation (14), each element of this vector denotes a decision variable of the optimization issue.

$$LB_x = Lp + Z_1 \times (Up - Lp); \qquad x = 1 : NBs \tag{14}$$

The bounds of the design parameters are *Up* and *Lp*, and Z_1 is a random d-dimensional vector containing uniformly distributed values inside the range [0,1]. At this point, LB_x records the location vector, x, of each bird.

3.2. Memory initialization

The proposed MLO algorithm incorporates memory-based learn search strategy (MBLSS) and diversity maintenance learn search strategy (DMLSS). These enhancements boost search efficiency by finding an equilibrium between localized exploitation and extensive issue space research. Every lyrebird's memory is upgraded to the MLO form after it has been saved.

$$LM_x = LB_x \qquad \forall\, x = 1 : NBs \tag{15}$$

where LM_k stores the initial location of each lyrebird, which is later used during the imitation process.

Equation (16) shows that the IAE function under optimization is used to determine each lyrebird's objective value (OF_x) after initialization.

$$OF_x = IAE\left(LB_x\right); \qquad x = 1 : NBs \tag{16}$$

The lyrebird with the lowest fitness score offers the greatest possible alternative (LY_{Best}) in the following ways, in accordance with the *IAE* minimization model:

$$LB_{Best} = arg\left(\min_{1<x<NBb}\left(OF_x\right)\right) \tag{17}$$

3.3. Improved phase of investigation using the suggested MBLSS

At this point, the LO algorithm exploits the natural inclination of lyrebirds to move to safer locations. Safe zones, which are continuously defined based on the optimization objective function, are the areas where other lyrebirds with higher fitness ratings are found. The safe zones of the kth lyrebird are expressed mathematically in the following manner:

$$Safe\_A_x = \left\{LB_i, OF_i \prec OF_x; \qquad i \in \left\{1 : NBs\right\}?\ x = 1 : NBs, i \neq x\right. \tag{18}$$

where $Safe\_A_x$ is the name of the group of safer locations that the x^{th} lyrebird can reach.

Each lyrebird regards individuals with higher fitness as potential guides, enabling it to navigate more effectively toward promising regions of the search space. This escape-based motion technique allows the lyrebird to move toward zones that perform better, increasing the algorithm's exploration capability by compelling search birds to visit previously unexplored regions of the solution environment. Selecting superior regions strategically directs the agents' exploration and prevents arbitrary search behavior. The new location of the k^{th} lyrebird is calculated by mathematically applying the next relation:

$$LB\_new_x = \begin{cases} LB_x & if \quad Safe\_A_x = \{\ \} \\ LB_x + z_a\left(Safer\_A_x - \left(I_x . LB_x\right)\right) & Else \end{cases} \tag{19}$$

where LB_x and LB_new_x are the present and projected location vectors for the xth lyrebird after the escape movement. $Safer\_A_x$ represents the randomly selected safe zone for the jth lyrebird from the collection ($Safe\_A_x$) provided by Equation (17). While z_a offers a random value that matches [0,1] and controls the trip in the direction of the secure zone, I_x consists of an arbitrarily selected integer that controls the impact of the current location during the entire updating procedure. In the event that no safe places are found for the x^{th} lyrebird, it remains where it is, as indicated by Equation (19).

The proposed MLO uses MBLSS to enhance the fleeing phase. Lyrebirds search for safe havens based on the best solutions currently accessible or on their more experienced colleagues. A

probabilistic imitation mechanism is provided that takes probability (*Pm*) into account.

$$LB\_new_x = LB_{Best} + Z_2 \times \left(LM_x - LB_x \right) \; if \; z_b < \alpha \tag{20}$$

where Z_2 illustrates a randomized vector of dimension (d), and z_b stands for a variable that is computed as follows:

$$\alpha = Pm \times \left({IT_n}/{IT_{n\,max}} \right) \tag{21}$$

where *Pm* indicates the imitation probability, and IT_n is the current iteration, while its maximum count is symbolized by (IT_{nmax}). This strategy improves local refinement by allowing the lyrebird to fortify previously viable locations through suggested MBLSS.

3.4. Enhanced phase of exploitation using the suggested DMLSS

Based on the lyrebird's innate hiding behavior, which involves concealing in a safe location to prevent predators from detecting it, the LO algorithm is being exploited at this stage. This behavior leads to a fine-tuning of the search in the area surrounding the current location. Hence, a stochastic updating mechanism is used to progressively change each lyrebird's position, becoming more cautious as the algorithm executes. Owing to this adaptive step-size mechanism, the initial iterations emphasize broader local exploration, whereas the later stages concentrate on intensified exploitation around promising regions. Throughout its exploitation, the potential location of the x^{th} lyrebird is ascertained using the following methodology:

$$LB\_new_x = LB_x + \left(1 - 2Z_3\right) \times \left(\frac{Up \; - \; Lp}{IT_n} \right) \tag{22}$$

where IT_n influences the current iteration count and the rate of progression. As it climbs, the step size gets smaller, encouraging more accurate local modifications.

Since DMLSS improves the hiding phase in the proposed MLO, the updating procedure in Equation (22) has been revised to reflect this:

$$LB\_new_x = \begin{cases} LB\_new_x = LB_x + \gamma \times \left(LB_{RD} - LB_x \right) & if \; Dis_x < \gamma \times Dis_{max} \\ LB_x + \left(1 - 2Z_3\right) \times \left(\dfrac{Up \; - \; Lp}{IT_n} \right) & Else \end{cases} \tag{23}$$

where Dis_x and Dis_{max} represent the crowding indicator and maximum distance across all lyrebirds as can be seen in Equations (24) and (25), respectively, while γ denotes the specified distance coefficient that is a component of the set [0,1], and LB_{RD} represents an arbitrarily selected lyrebird that is not the current x^{th} bird. This creates a regulated extension in seeking space, which facilitates exploring new places and escaping congested areas.

$$Dis_x = \frac{\sum_{j=1}^{NBs} \left\| LB_x - LB_j \right\|}{NBs} \tag{24}$$

$$Dis_{max} = \max_{j,x} \left\| LB_j - LB_x \right\| \tag{25}$$

As demonstrated, the x^h lyrebird's proximity to the rest of the population is determined by the crowding index Dis_x; a lower Dis_x suggests the agent is in a congested (perhaps stagnant) area. However, Dis_{max} calculates the greatest Euclidean distance between any two of the population's lyrebirds.

3.5. Updates to the locations and recollections of the bird

The associated fitness rating (OF_new_x) is evaluated using the target function after the changed location (LB_new_x) has been determined. If this new objective number reveals an enhancement over the current situation, the current position is modified:

$$LB_x\left(IT_n+1\right) = \begin{cases} LB\_new_x & OF\_new_{:} \le OF_x \\ LB_x\left(IT_n\right) & Else \end{cases} \tag{26}$$

In addition, their combined memories have been updated. Each lyrebird's memory is updated only as its fitness increases in order to maintain accuracy and adaptability:

$$LM_x\left(IT_n+1\right) = \begin{cases} LB\_new_x & OF\_new_{:} \le OF_x \\ LM_x\left(IT_n\right) & Else \end{cases} \tag{27}$$

The suggested MLO design ensures that the memory preserves the most famous history of the lyrebird. The MLO stages are depicted in Figure 4.

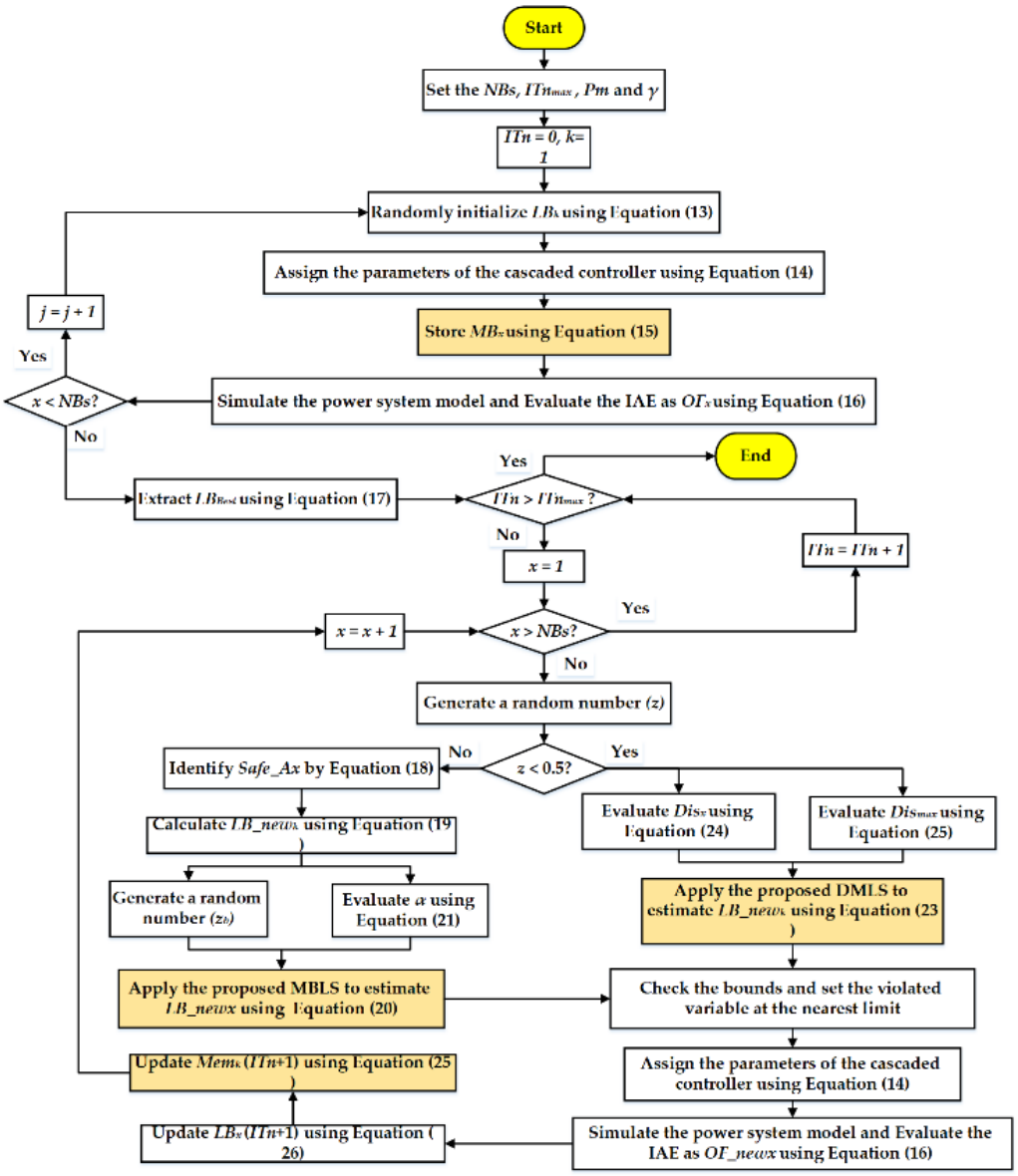

Figure 4. Proposed MLO steps.

4. Results and discussion

The proposed MLO and LO methods are evaluated using three case studies: the RTC France solar cell, the MSX-60, and the Shell S75 PV modules. In the first case, the commercial RTC France silicon solar cell operates at 33 °C under an irradiance of 1000 W/m². Its electrical characteristics include a short-circuit current of 0.7605 A, an open-circuit voltage of 0.5727 V, and a maximum power point defined by 0.4590 V and 0.6755 A. The second case examines the MSX-60 polycrystalline silicon PV module, which consists of 36 series-connected cells. The third case examines the Shell S75 monocrystalline silicon PV module, which consists of 36 series-connected cells.

Table 1 presents the lower and upper bounds of the parameters for the MSX–60 PV module and the RTC France solar cell. Based on the experimental I–V data, this section provides the parameter identification results for the SD, DD, and TD models of the solar systems.

Table 1. Boundaries of parameters for SD, DD, and TD PV models.

Parameter	RTC France solar cell		MSX–60 PV module		Shell S75	
	Lower	Upper	Lower	Upper	Lower	Upper
I_{ph} (A)	0.00	10.00	3.5	4	0.00	20.00
R_{Sh} (Ω)	0.00	100.00	150	3000	0.00	1000.00
I_{S1}, I_{S2}, and I_{S3} (μA)	0.00	10.00	0.01	1	0.00	1000.00
η_1, η_2, and η_3 per cell	1.00	2.00	1.00	2.00	1.00	2.00
R_S (Ω)	0.00	2.00	0.2	0.4	0.00	5.00
No series cells (*Nc*)	1		36		36	
Open circuit voltage (*Voc*)	0.5727 V		21.10 V		21.60 V	
Maximum power (*Pmax*)	0.323 W		60 W		75	
Voltage at Pmax (*Vm*)	0.4590 V		17.10 V		17.60 V	
Current at Pmax (*Im*)	0.6755 A		3.50 A		4.26 A	

Additionally, the control parameters used for the proposed MLO algorithm are summarized in Table 2. A population size of 100 search agents and a maximum of 1000 iterations were selected to ensure a sufficient balance between computational cost and convergence reliability [53]. The imitation probability $Pm = 0.5$ regulates the likelihood of adopting experience from better-performing solutions, while the distance coefficient $\gamma = 0.25$ in Eq. (23) governs the diversity preservation mechanism during exploitation. A fixed random seed (Mersenne Twister, seed = 0) is used to guarantee result reproducibility. The algorithm terminates when the maximum iteration count is reached, as no additional convergence-based stopping criterion is required due to the strong stability observed across repeated independent runs. Runs denote the number of independent executions of the optimizer performed to account for its randomized behavior.

Table 2. Control parameters of the proposed MLO.

Control parameter	Value
NBs (population size)	100
IT_{nmax} maximum iterations	1000
IT_n	A counter starting from 1 to IT_{nmax}
Pm [imitation probability, Eq. (21)]	0.5
γ [distance coefficient used in Eq. (23)]	0.25
random seeds	A random number seed using the default algorithm "Mersenne Twister generator" with seed 0.
stopping criteria	When the maximum iteration count (IT_{nmax}) is reached

4.1. The MSX–60 PV module

4.1.1. SD model

The SD model features of the MSX–60 PV module are extracted using the suggested MLO. Table 3 lists the five unidentified SD parameter values for different inspired techniques that yielded the best experiment outcomes. Besides, the table lists the evaluated parameters of the suggested MLO, which

are 1 for the ideality factor for d1, 6.8929271 Ω for shunt resistance, 0.008009809 Ω for series resistance, 3.803241225A for photo-current, and 1.21876×10^{-2} μA for saturation current for d1. In PV modeling, ideality factors close to 1 typically represent dominant recombination in the quasi-neutral region, while values near 2 are associated with recombination in depletion regions. Therefore, the occurrence of η values near these limits is physically meaningful and consistent with well-reported semiconductor behavior. Furthermore, the bounds were selected based on established PV modeling literature to avoid identifiability issues and unrealistic parameter growth. Nonetheless, we have now added a short explanatory note in the manuscript to clarify the physical interpretation of these parameter values and to confirm that their convergence to bounds does not indicate over-constraining but reflects plausible diode recombination mechanisms.

The results show that the proposed MLO outperforms the conventional LO in terms of competitiveness. The proposed MLO achieves a desirable RMSE value of 1.74806×10^{-3}, which is lower than the conventional LO at 4.39308×10^{-3}. Additionally, the table displays MLO's max, mean, and standard deviation values of 1.74810×10^{-3}, 1.74806×10^{-3}, and 5.61686×10^{-9}, respectively. When compared to the conventional LO, the acquired results reveal that the MLO significantly improves accuracy and efficacy for the best SD model characterization. The ideal parameters for the solar PV model under discussion are found after about 50 independent runs. Figure 5 offers a statistical summary of the RMSE values for both algorithms and the SD model throughout the 50 runs to further examine the algorithm's robustness. It can be seen from the figure that the proposed MLO provides higher robustness than the conventional LO.

Figure 6 illustrates the convergence graphs of the proposed MLO and the conventional LO for the SD PV model of the MSX-60 module. Figure 6 confirms that the proposed MLO from the beginning of the iterative journey is associated with significant progress.

Table 3. Electrical parameters obtained by the suggested MLO and LO for the SD model.

	LO	MLO
Iph	3.794200555	3.803241225
Rs	0.007976533	0.008009809
Rsh	8.381544154	6.8929271
Io1	1.35057E-08	1.21876E-08
n1	1.005237573	1
min	4.39308E-03	1.74806E-03
mean	8.55766E-03	1.74806E-03
max	1.27844E-02	1.74810E-03
Std	2.18006E-03	5.61686E-09

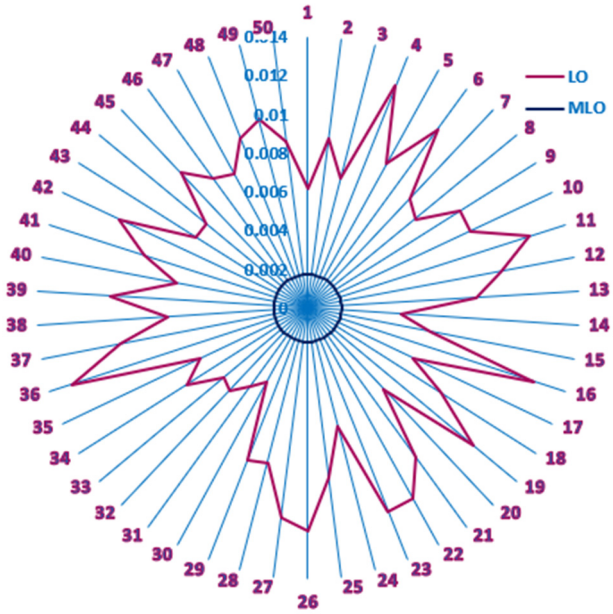

Figure 5. 50 runs of the proposed MLO and the conventional LO for the SD PV model of MSX-60.

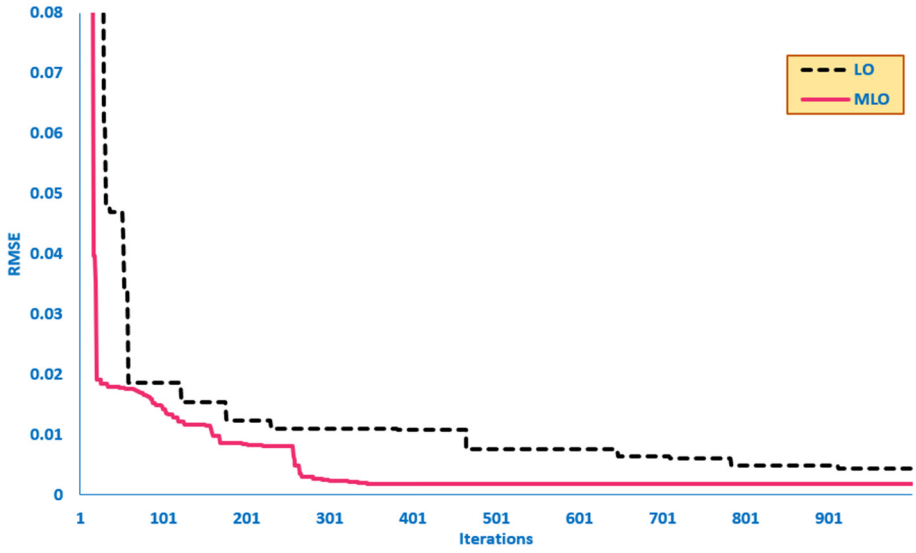

Figure 6. Convergence graphs of the proposed MLO and the conventional LO for the SD PV model of MSX-60.

The observed and simulated I–V and P–V features for the SD model of MSX-60 can be seen in Figure 7(a, b). The suggested MLO and the traditional LO are used to represent the 15 measured points for this module. The data produced by the MLO approach appears to closely match the data obtained through experimentation, indicating that the MLO technique became effective in generating power and current across a spectrum of voltage settings. The simulated and measured absolute errors of power vary from 0 to 7.5767×10^{-2}, whereas the simulated and measured current absolute errors vary from 8.37347×10^{-9} to 1.7523×10^{-5}, as demonstrated in Figure 8(a, b) and Table 4.

Table 4. Absolute differences between the proposed MLO's simulated and experimental currents and powers for the MSX-60 SD PV model.

No.	Vexp	Iexp	Isim	Pexp	Psim
1	0	3.8	3.798826	0	0
2	1.6	3.7932	3.792386	6.06912	6.067817
3	3.1	3.7868	3.786348	11.73908	11.73768
4	4.6	3.7804	3.780308	17.38984	17.38942
5	6.1	3.774	3.774264	23.0214	23.02301
6	7.6	3.7676	3.768198	28.63376	28.63831
7	9.1	3.761	3.762047	34.2251	34.23463
8	10.6	3.7542	3.755554	39.79452	39.80888
9	12.1	3.7461	3.747695	45.32781	45.34711
10	13.6	3.7327	3.734383	50.76472	50.78761
11	15.1	3.6987	3.699491	55.85037	55.86231
12	17.1	3.5	3.497037	59.85	59.79934
13	18.1	3.189	3.184814	57.7209	57.64513
14	19.6	2.0962	2.098981	41.08552	41.14002
15	21.1	0	−0.00043	0	−0.00911
No.	IAE	PAE	Absolut IAE	Absolut PAE	
1	−0.00117434	0	1.37908E-06	0	
2	−0.00081442	0.00130307	6.63277E-07	0.001303069	
3	−0.0004523	0.00140212	2.04572E-07	0.00140212	
4	−9.1507E-05	0.00042093	8.37347E-09	0.000420931	
5	0.000263953	−0.0016101	6.96714E-08	0.001610116	
6	0.000598076	−0.0045454	3.57695E-07	0.004545378	
7	0.001047018	−0.0095279	1.09625E-06	0.009527866	
8	0.001354308	−0.0143557	1.83415E-06	0.01435566	
9	0.001595418	−0.0193046	2.54536E-06	0.019304554	
10	0.00168343	−0.0228947	2.83394E-06	0.022894654	
11	0.00079055	−0.0119373	6.2497E-07	0.011937308	
12	−0.00296267	0.05066171	8.77743E-06	0.050661707	
13	−0.00418605	0.07576747	1.7523E-05	0.075767474	
14	0.002780604	−0.0544998	7.73176E-06	0.054499844	
15	−0.0004316	0.00910677	1.86279E-07	0.009106768	

Figure 7(a, b) illustrates the observed and simulated I–V and P–V characteristics of the SD model for the MSX-60 module. Both the proposed MLO and the conventional LO methods are applied to represent the 15 measured data points for this module. The results indicate that the MLO-based simulation closely aligns with the experimental data, confirming the effectiveness of MLO in accurately predicting power and current over a range of voltage values. The absolute error between simulated and measured power ranges from 0 to 7.5767×10^{-2}, and the current absolute error varies between 8.37×10^{-9} and 1.75×10^{-5}, as shown in Figure 8(a, b) and summarized in Table 4.

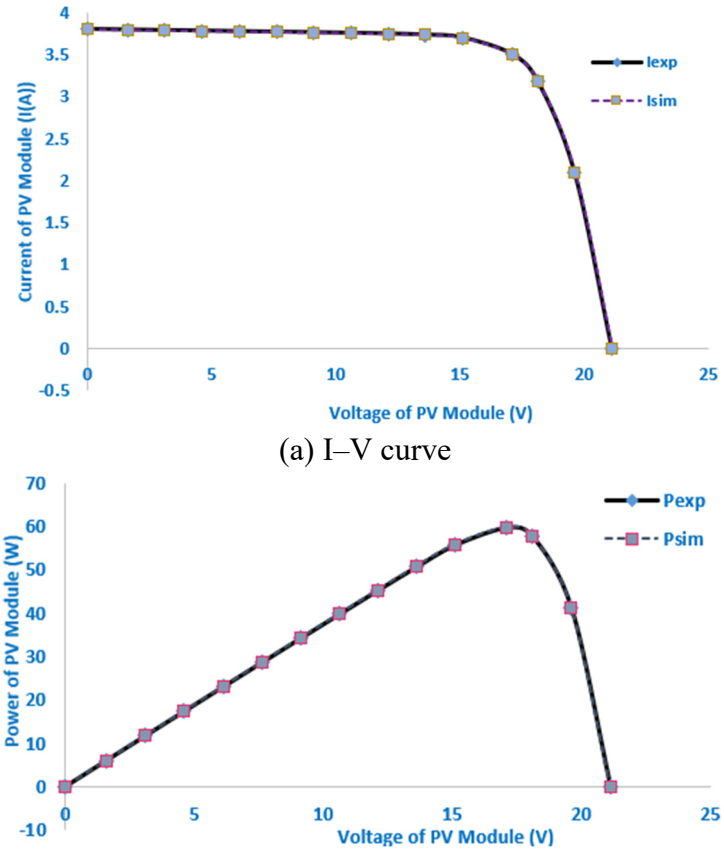

(a) I–V curve

(b) P–V curve

Figure 7. Characteristic curves of the solar modules, both measured and estimated for the MSX-60 SD PV model.

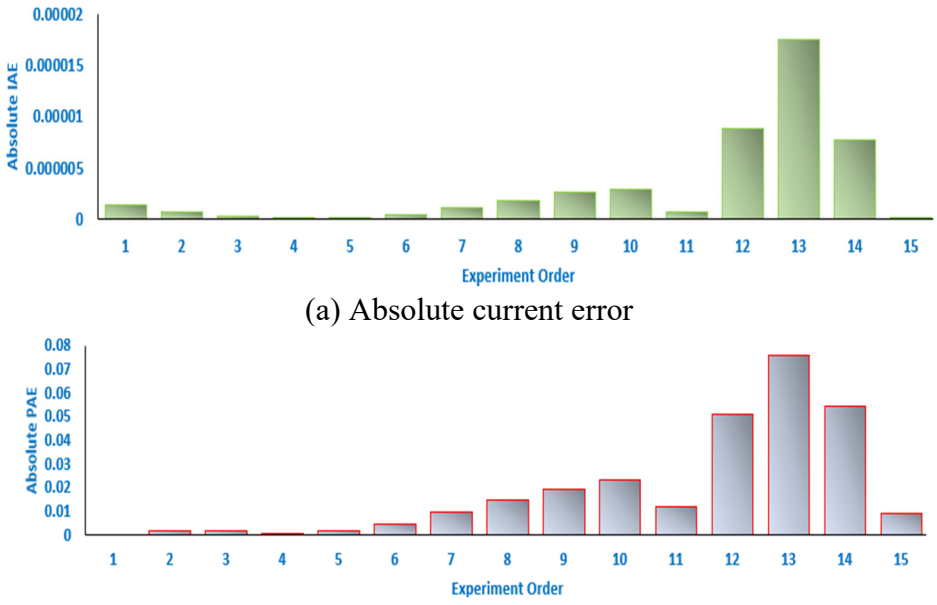

(a) Absolute current error

(b) Absolute power error

Figure 8. Absolute errors in the currents and powers between simulated and experimental values of the MSX-60 SD PV model.

4.1.2. DD model

The DD model features of the MSX–60 PV module are extracted using the suggested MLO. Table 5 lists the seven unidentified DD parameter values for different inspired techniques that yielded the best experiment outcomes. Besides, the table lists the evaluated parameters of the suggested MLO, which are 1 and 1 for the ideality factor for d1 and d2, 6.892926882 Ω for shunt resistance, 0.008009809 Ω for series resistance, 3.803241226 A for photo-current, and 1.21876×10^{-2} μA and 0 μA for saturation current for d1 and d2. This demonstrates that the proposed MLO achieves a desirable RMSE value of 1.74806×10^{-3}, which is lower than that of the conventional LO, at 4.04117×10^{-3}. The results show that the proposed MLO outperforms the conventional LO in terms of competitiveness. Additionally, the proposed MLO outperforms corresponding approaches in terms of competitiveness, including the analytical methods (AM) [54], mountain-climbing algorithm (MCA) [55], Newton–Raphson method (NRM) [56], and a combination of a numerical approach with a slope adjustment technique (NASAT) [57]. Moreover, the table displays the MLO's max, mean, and standard deviation values: 1.78001×10^{-3}, 1.74873×10^{-3}, and 4.51735×10^{-6}, respectively. When compared to the conventional LO, the MLO significantly improves accuracy and efficacy for the best DD model characterization. The ideal parameters for the solar PV model under discussion are found after about 50 independent runs. Figure 9 offers a statistical summary of the RMSE values for both algorithms and the DD model throughout the 50 runs in order to further examine the algorithm's robustness. It can be seen from the figure that the proposed MLO provides higher robustness than the conventional LO.

Table 5. Electrical parameters obtained by the suggested MLO and LO for the DD model.

	AM [54]	MCA [55]	NRM [56]	NASAT [57]	LO	MLO
Iph	3.8046	3.808361	3.8084	3.8618	3.796545747	3.803241226
Rs	0.3397	0.372046	0.3692	0.2904	0.008078825	0.008009809
Rsh	280.2171	169.081308	169.0471	286.1209	8.537603576	6.892926882
Io1	4.033E- 06	4.597752E- 10	6.1528E-10	3.1092E-06	0	1.21876E-08
n_1	2.0014	2	1.9997	2	1	1
Io2	3.9901E-10	4.597752E-10	4.8723E-10	6.0842E-10	1.22295E-08	0
n2	0.99859	1	1.0003	1	1	1
min	**1.908 E-01**	**1.666 E-01**	**1.379 E-01**	**3.43 E-02**	**4.04117E-03**	**1.74806E-03**
Mean	-	-	-	-	7.70284E-03	1.74873E-03
max	-	-	-	-	1.10606E-02	1.78001E-03
Std	-	-	-	-	1.77743E-03	4.51735E-06

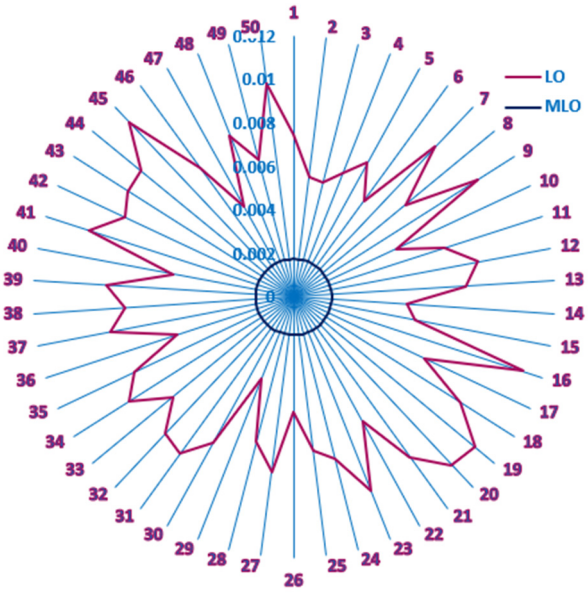

Figure 9. 50 runs of the proposed MLO and the conventional LO for the DD PV model of MSX-60.

Figure 10 illustrates the convergence graphs of the proposed MLO and the conventional LO for the DD PV model of the MSX-60 module. Figure 10 confirms that the proposed MLO from the beginning of the iterative journey is associated with significant progress. This is due to an improvement in the exploration capability made possible by the MLO approach. The improvement starts at iteration 100 for all three models with the best converging attributes.

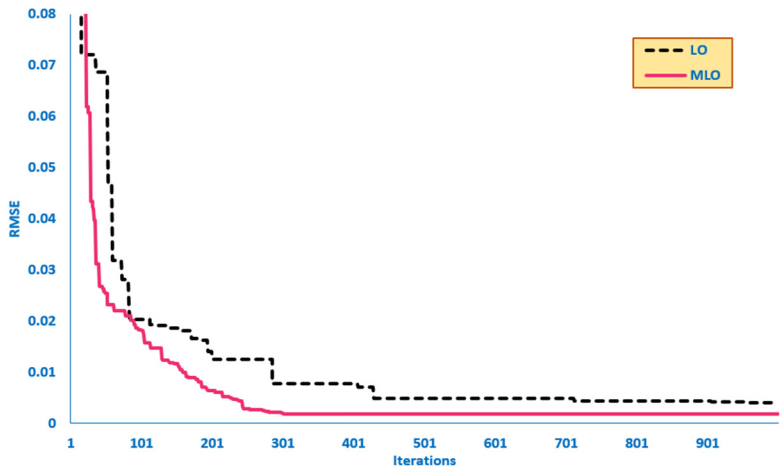

Figure 10. Convergence graphs of the proposed MLO and the conventional LO for the DD PV model of MSX-60.

Figure 11(a, b) shows the measured and simulated I–V and P–V curves for the DD model of the MSX-60 module. The MLO-generated results exhibit a close agreement with the experimental data, demonstrating the method's accuracy in predicting power and current across different voltage ranges. The absolute error between simulated and measured power lies between 0 and 7.5768×10^{-2}, while the error for current ranges from 8.38559×10^{-9} to 1.7523×10^{-5}, as demonstrated in Figure 12(a, b) and Table 6.

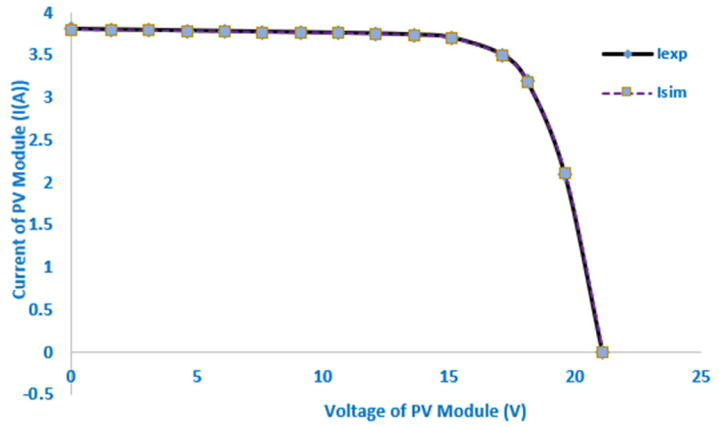

(a) I–V

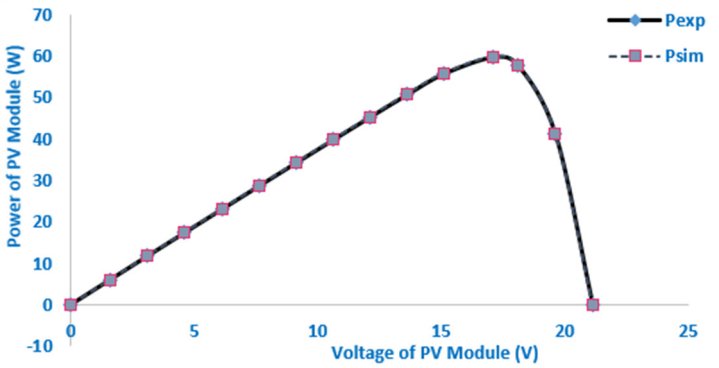

(b) P–V curve

Figure 11. Characteristic curves of the solar modules, both measured and estimated for the MSX-60 DD PV model.

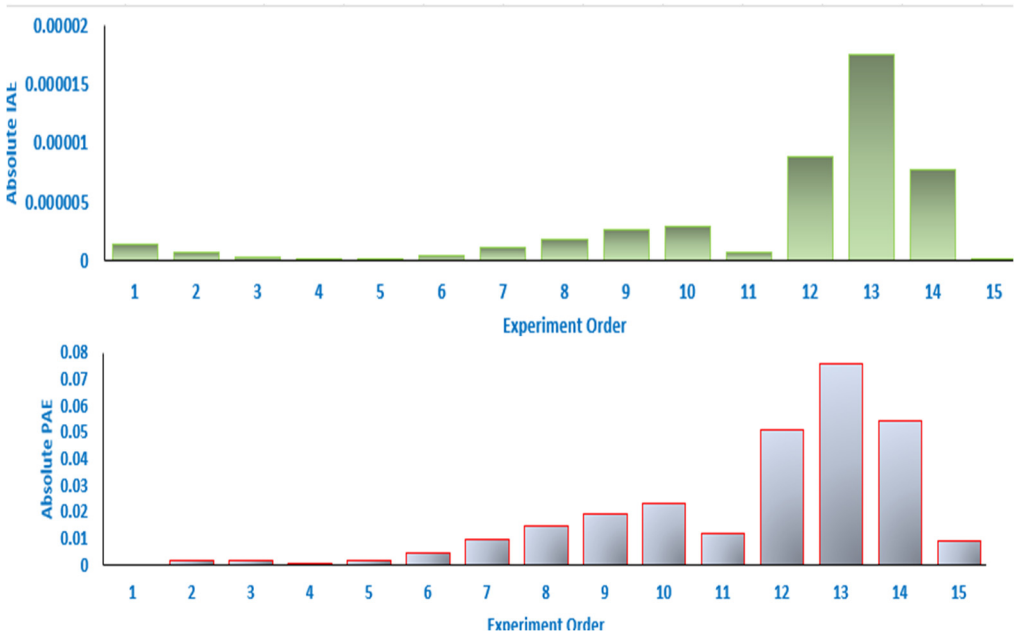

Figure 12. Absolute errors in the currents and powers between simulated and experimental values of the MSX-60 SD PV model.

Table 6. Absolute differences among the proposed MLO's simulated and experimental currents and powers for the MSX-60 DD PV model.

	Vexp	Iexp	Isim	Pexp	Psim
1	0	3.8	3.798826	0	0
2	1.6	3.7932	3.792385	6.06912	6.067817
3	3.1	3.7868	3.786348	11.73908	11.73768
4	4.6	3.7804	3.780308	17.38984	17.38942
5	6.1	3.774	3.774264	23.0214	23.02301
6	7.6	3.7676	3.768198	28.63376	28.63831
7	9.1	3.761	3.762047	34.2251	34.23463
8	10.6	3.7542	3.755554	39.79452	39.80888
9	12.1	3.7461	3.747695	45.32781	45.34712
10	13.6	3.7327	3.734384	50.76472	50.78762
11	15.1	3.6987	3.699491	55.85037	55.86231
12	17.1	3.5	3.497037	59.85	59.79934
13	18.1	3.189	3.184814	57.7209	57.64513
14	19.6	2.0962	2.09898	41.08552	41.14002
15	21.1	0	−0.00043	0	−0.0091
	IAE	PAE	Absolut IAE	Absolut PAE	
1	−0.0011745	0	1.37944E-06	0	
2	−0.00081454	0.00130327	6.63479E-07	0.001303267	
3	−0.00045239	0.00140241	2.04658E-07	0.001402415	
4	−9.1573E-05	0.00042124	8.38559E-09	0.000421235	
5	0.000263916	−0.0016099	6.96517E-08	0.001609888	
6	0.000598067	−0.0045453	3.57685E-07	0.004545312	
7	0.001047038	−0.009528	1.09629E-06	0.009528048	
8	0.001354356	−0.0143562	1.83428E-06	0.014356175	
9	0.001595494	−0.0193055	2.5456E-06	0.019305479	
10	0.001683532	−0.022896	2.83428E-06	0.022896038	
11	0.000790667	−0.0119391	6.25154E-07	0.01193907	
12	−0.00296261	0.05066055	8.77703E-06	0.05066055	
13	−0.00418608	0.07576806	1.75233E-05	0.075768064	
14	0.002780369	−0.0544952	7.73045E-06	0.054495236	
15	−0.00043144	0.0091033	1.86137E-07	0.009103299	

4.1.3. TD model

The TD model features of the MSX–60 PV module are extracted using the suggested MLO. Table 7 lists the nine unidentified TD parameter values for different inspired techniques that yielded the best experiment outcomes. Besides, the table lists the evaluated parameters of the suggested MLO, which are 1, 1, and 1 for the ideality factor for d1, d2, and d3, 6.892926994 Ω for shunt resistance, 0.008009809 Ω for series resistance, 3.803241225 A for photo-current, and 0, 1.21876×10^{-2} μA and 0 μA for saturation current for d1, d2, and d3.

The results show that the proposed MLO outperforms the conventional LO in terms of competitiveness. This demonstrates that the proposed MLO achieves a desirable RMSE value of 1.74806×10^{-3}, lower than that of the conventional LO at 3.22789×10^{-3}. Additionally, the table displays the MLO's max, mean, and standard deviation values: 1.97327×10^{-3}, 1.75887×10^{-3}, and 3.83808×10^{-5}, respectively. When compared to the conventional LO, the acquired results reveal that the MLO significantly improves accuracy and efficacy for the best TD model characterization. The ideal parameters for the solar PV model under discussion are found after about 50 independent runs. Figure 13 offers a statistical summary of the RMSE values for both algorithms and the TD model throughout the 50 runs in order to further examine the algorithm's robustness. It can be seen from the figure that the proposed MLO provides higher robustness than the conventional LO.

Table 7. Electrical parameters obtained by the suggested MLO and LO for the TD model.

	LO	MLO
Iph	3.803742788	3.803241225
Rs	0.007860924	0.008009809
Rsh	7.162340399	6.892926994
Io1	6.97299E-09	0
n1	1.109662637	1
Io2	1.10214E-08	1.21876E-08
n2	1.002642904	1
Io3	7.5425E-10	0
n3	1.001484974	1
min	**3.22789E-03**	**1.74806E-03**
mean	**7.65579E-03**	**1.75887E-03**
max	**1.14736E-02**	**1.97327E-03**
Std	**1.70209E-03**	**3.83808E-05**

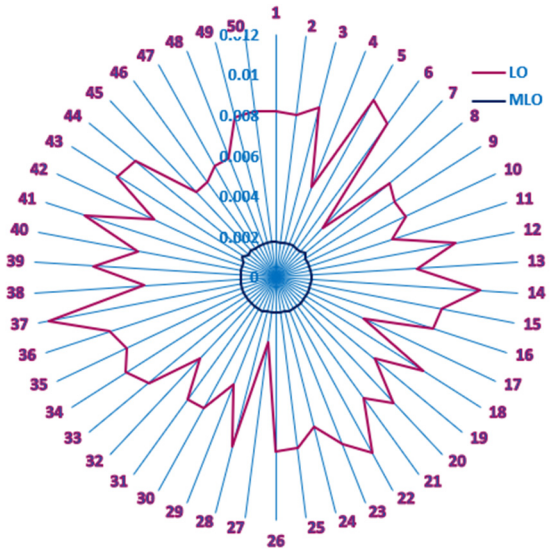

Figure 13. 50 runs of the proposed MLO and the conventional LO for the TD PV model of MSX-60.

Moreover, Figure 14 illustrates the convergence graphs of the proposed MLO and the conventional LO for the TD PV model of the MSX-60 module. Figure 14 confirms that the proposed MLO from the beginning of the iterative journey is associated with significant progress. This is due to an improvement in the exploration capability made possible by the MLO approach. The improvement starts at iteration 180 for all three models with the best converging attributes.

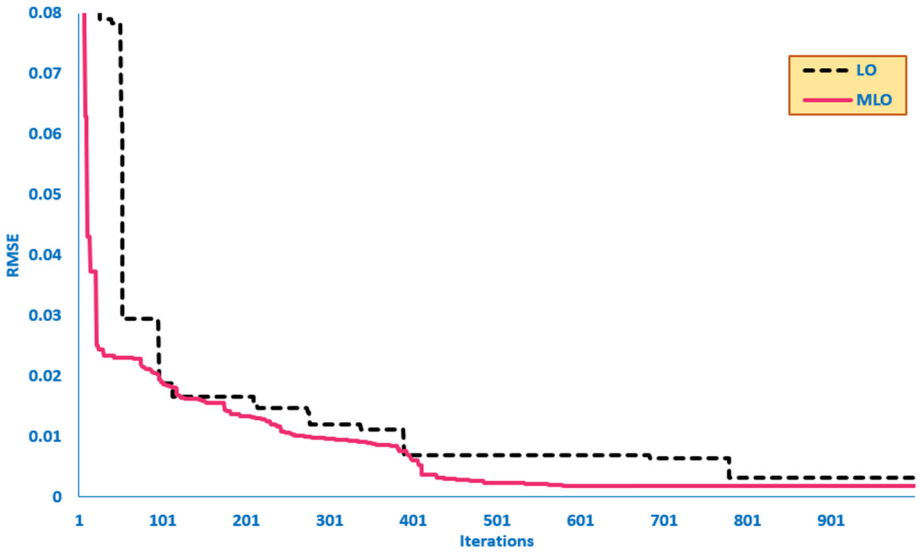

Figure 14. Convergence graphs of the proposed MLO and the conventional LO for the TD PV model of MSX-60.

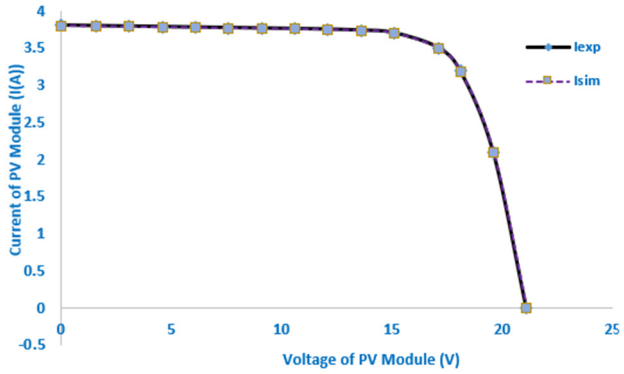

(a) I-V

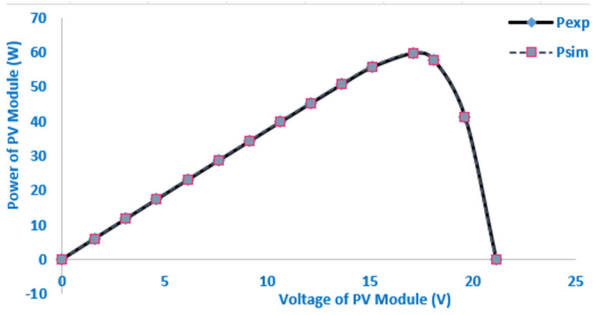

(b) P-V curve

Figure 15. Characteristic curves of the solar modules, both measured and estimated.

Moreover, Figure 15(a, b) displays the experimental and simulated I–V and P–V curves for the TD model of the MSX-60 module. The results generated by the MLO method show strong agreement with the experimental measurements, highlighting its capability to accurately predict power and current across various voltage levels. The absolute error for power ranges from 0 to 7.5339×10^{-2}, and the error for current varies between 2.22984×10^{-8} and 1.7326×10^{-5}, as demonstrated in Figure 16(a, b) and Table 8.

Table 8. Absolute differences between the proposed MLO's simulated and experimental currents and powers for the MSX-60 TD PV model.

	Vexp	Iexp	Isim	Pexp	Psim
1	0	3.8	3.798538	0	0
2	1.6	3.7932	3.792144	6.06912	6.06743
3	3.1	3.7868	3.786148	11.73908	11.73706
4	4.6	3.7804	3.780151	17.38984	17.3887
5	6.1	3.774	3.774149	23.0214	23.02231
6	7.6	3.7676	3.768126	28.63376	28.63776
7	9.1	3.761	3.762017	34.2251	34.23436
8	10.6	3.7542	3.755567	39.79452	39.80901
9	12.1	3.7461	3.747749	45.32781	45.34777
10	13.6	3.7327	3.734477	50.76472	50.78888
11	15.1	3.6987	3.699614	55.85037	55.86417
12	17.1	3.5	3.49714	59.85	59.80109
13	18.1	3.189	3.184838	57.7209	57.64556
14	19.6	2.0962	2.098811	41.08552	41.1367
15	21.1	0	-0.00041	0	−0.00875
	IAE	PAE	Absolut IAE	Absolut PAE	
1	−0.00146153	0	2.13606E-06	0	
2	−0.00105634	0.00169014	1.11586E-06	0.001690145	
3	−0.00065179	0.00202054	4.24825E-07	0.002020537	
4	−0.00024856	0.00114339	6.17839E-08	0.001143393	
5	0.000149326	−0.0009109	2.22984E-08	0.000910891	
6	0.000525869	−0.0039966	2.76538E-07	0.003996605	
7	0.001017192	−0.0092564	1.03468E-06	0.009256443	
8	0.001366709	−0.0144871	1.86789E-06	0.014487114	
9	0.001649444	−0.0199583	2.72066E-06	0.019958269	
10	0.001776716	−0.0241633	3.15672E-06	0.024163344	
11	0.000913975	−0.013801	8.3535E-07	0.013801019	
12	−0.00286008	0.04890731	8.18004E-06	0.048907314	
13	−0.0041624	0.07533939	1.73255E-05	0.075339385	
14	0.002611172	−0.051179	6.81822E-06	0.051178965	
15	−0.00041465	0.00874916	1.71936E-07	0.008749161	

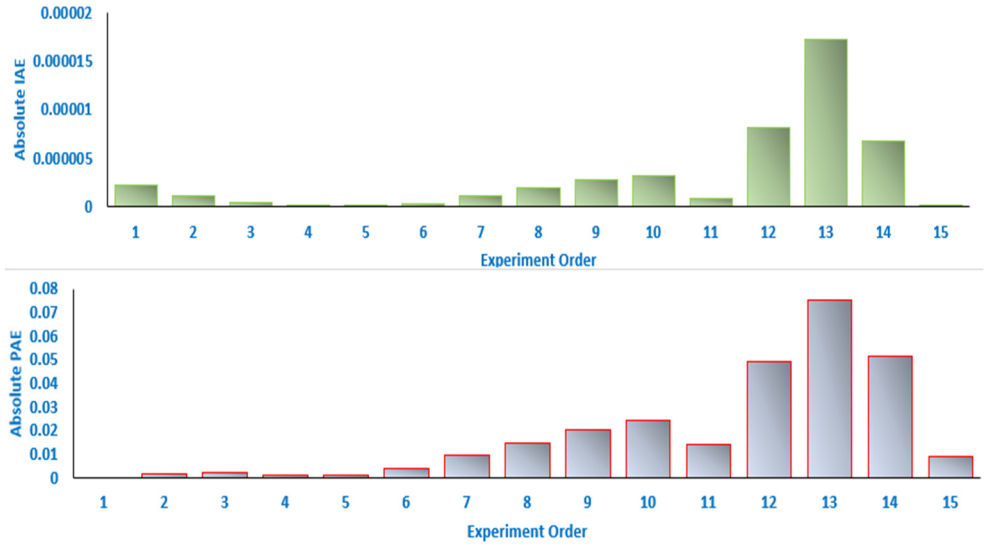

Figure 16. Absolute errors in the currents and powers between simulated and experimental values of the MSX-60 SD PV model.

4.1.4. Computational budget and runtime discussion considering TD model

Both LO and the proposed MLO algorithms were executed under an identical computational budget to ensure a fair comparison. Table 9 displays the computational budget and runtime comparison for the MSX-60 TD PV model. As shown, each algorithm utilized a population size of 100 solutions and was iterated for 1000 iterations, resulting in a total of 100,000 function evaluations per run. This equal evaluation budget allows performance differences to be attributed solely to algorithmic design rather than unequal search effort. The average CPU runtime measured in MATLAB (R2017b) on a machine with 8 GB RAM was approximately 38.58 seconds for the conventional LO and 57.70 seconds for the proposed MLO. The slightly higher computational time for MLO is expected, as the additional memory-based and diversity maintenance mechanisms introduce extra computational operations in both exploration and exploitation phases. However, this increase in runtime is modest and justified by the significant improvements in accuracy, convergence behavior, and robustness, as demonstrated by the lower RMSE values and reduced standard deviation across multiple runs. Therefore, despite a ~50% increase in CPU time, the performance benefits of MLO outweigh its computational overhead, making it computationally efficient and scalable for real PV parameter estimation problems.

Table 9. Computational budget and runtime comparison for the MSX-60 TD PV model.

Item	LO algorithm	MLO algorithm
Population size (*NBs*)	100	100
Maximum iterations (IT_{nmax})	1000	1000
Total function evaluations	100,000	100,000
CPU elapsed time (s)	38.58 s	57.70 s
MATLAB memory usage	1778 MB	1798 MB
Maximum available RAM	8085 MB	8085 MB

4.2. Application for the RTC France solar cell

4.2.1. SD model

The SD model features of the RTC France solar cell are extracted using the suggested MLO. Table 10 lists the five unidentified SD parameter values for different inspired techniques that yielded the best experiment outcomes. The results show that the proposed MLO outperforms corresponding approaches in terms of competitiveness. This demonstrates that the proposed MLO achieves a desirable RMSE value of 9.86022×10^{-4}. Additionally, the table displays the electrical parameters that were generated from PV utilizing recognized optimization methods, including the classified perturbation mutation marine predator algorithm (MPA) [58], barnacles mating optimizer (BMA) [59], PSO (CPMPSO) [60], ant lion optimizer (ALO) [61], RIME [53], a performance-guided JAYA (PGJAYA) [62], enhanced MPA (EMPA) [58], enriched Harris hawks optimization (EHHO) [35], growth optimizer (GO) [63], material generation algorithm (MGA) [64], neighborhood scheme-based Laplacian MBA (NLBMA) [65], lightning attachment procedure optimization (LAPO) [66], flexible PSO (FPSO) [67], multi-verse optimizer (MVO) [68], jellyfish search (JFS) optimizer [58], equilibrium optimizer (EO) [58], hybrid PSO–GWO algorithm (PSOGWO) [69], hybrid firefly and pattern search (HFAPS) [70], HEAP optimizer [58], and particle swarm optimization (PSO) [71].

Besides, the table lists the evaluated parameters of the suggested MLO, which are 1.483914803 for the ideality factor for d1, 17.04778813 Ω for shunt resistance, 0.005601219 Ω for series resistance, 1.663749645 A for photo-current, and 3.31823×10^{-1} μA for saturation current.

Table 10. Electrical parameters obtained by the suggested MLO and LO for the SD model.

Algorithm	I_{ph} (A)	I_{sd} (μA)	n	R_{sh} (Ω)	R_{ss} (Ω)	*RMSE*
MLO	1.663749645	6.0068	1.876730845	17.04778813	0.005601219	**9.86022E-04**
LO	0.760827451	3.31823E-01	1.483914803	53.96055333	0.036279447	**9.89674E-04**
RIME[53]	0.760776	3.23021×10^{-1}	1.481184	53.71865291	0.036377096	9.9755×10^{-4}
MGA [64]	0.760776	3.23×10^{-1}	1.481184	53.71852	0.036377	9.8602×10^{-4}
EO [58]	8.209153	2.85×10^{-2}	1.218068	7.714703	0.004815	2.888×10^{-3}
PGJAYA [62]	8.2167	0.002284	58.1742	773.8117	0.3435	1.5455×10^{-4}
MPA[58]	8.184927	7.94459×10^{-2}	1.285180059	92.14823504	0.004537611	1.487×10^{-2}
FPSO [67]	8.2186	0.001436	56.9854	130.2813	0.2409	2.8214×10^{-2}
PSOGWO [69]	8.2132	9.6768	1.7463	38.8968	0.0011	1.2700×10^{-1}
GO [63]	8.192967	4.31808×10^{-2}	1.244346	15.103921	0.004710	8.515347×10^{-3}
PSO [71]	8.2027	2.8852	1.6052	33.8855	0.0019	1.0195×10^{-1}
JFS [58]	8.193182	4.72×10^{-2}	1.250052	14.97462	0.004679	9.477×10^{-3}
CPMPSO[60]	8.21689146	0.00224195	1.07641028	763.535149	0.34381405	1.53903×10^{-3}
EHHO [35]	8.2224	0.000001	80.6915	1806.0252	0.1835	5.9507×10^{-2}
HFAPS[70]	8.1992	0.154161	74.5795	1448.2590	0.2396	4.9863×10^{-2}
MVO [68]	8.2527	0.063908	69.2388	134.4813	0.1341	8.3800×10^{-2}
HEAP [58]	8.200974	4.49×10^{-2}	1.246924	11.87468	0.004696	7.425×10^{-3}
NLBMA [65]	8.1467	0.0022	1.0839	5.0000	0.0045	3.3610×10^{-2}
LAPO [66]	8.2155	8.1491	1.7258	5.0000	0.001	1.3813×10^{-1}
BMA [59]	8.1950	3.1015	1.6130	100.0000	0.0019	1.0244×10^{-1}
EMPA [58]	8.21195	3.59×10^{-2}	1.232551	7.560713	0.004742	3.847×10^{-3}

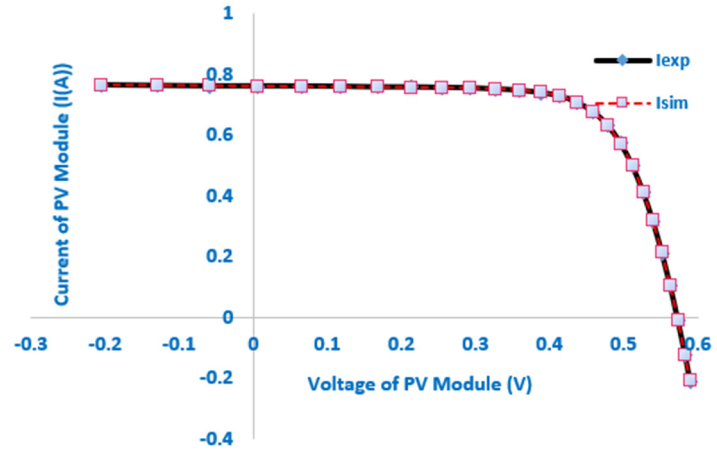

(a) I–V

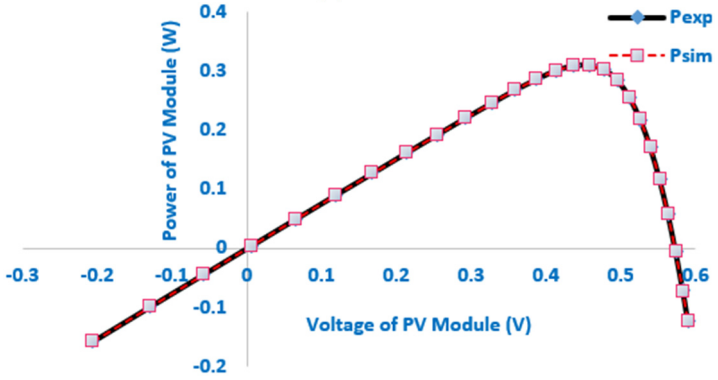

(b) P–V curve

Figure 17. Characteristic curves for RTC France SD PV cell, both measured and estimated.

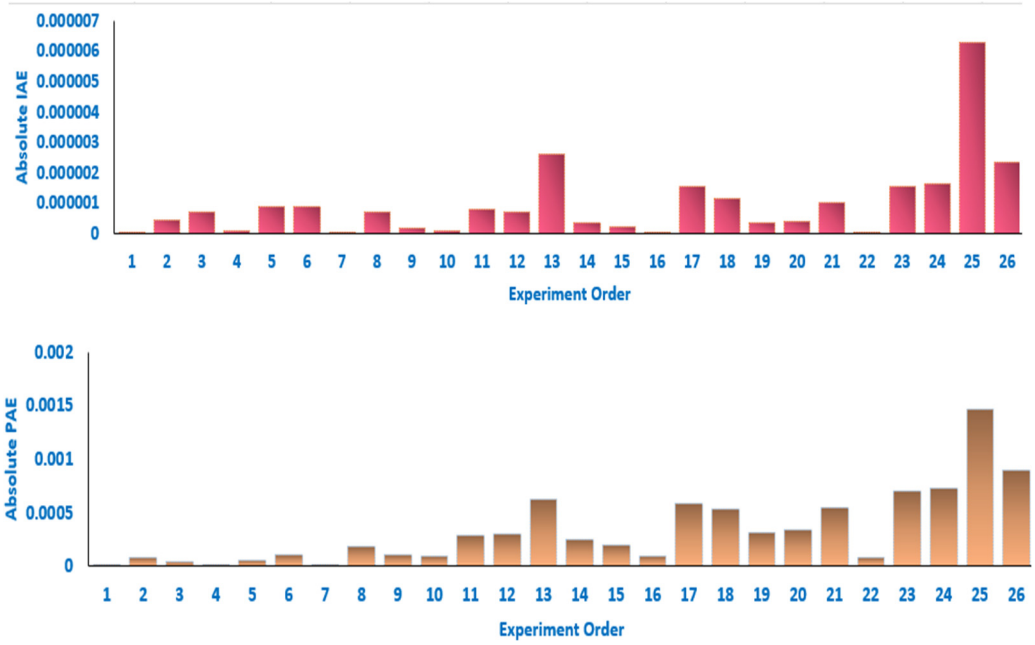

Figure 18. Absolute errors in the currents and powers between simulated and experimental values of the RTC France SD PV cell.

Furthermore, Figure 17(a, b) presents the experimental and simulated I–V and P–V curves for the SD model of the RTC France PV cell. The results obtained using the MLO approach show a strong correlation with the experimental data, confirming its effectiveness in accurately estimating power and current across different voltage levels. The absolute error for power ranges from 1.97222×10^{-6} to 1.4626×10^{-3}, while the error for current varies between 7.69491×10^{-9} and 6.287×10^{-6}, as illustrated in Figure 18(a, b).

4.2.2. DD model

The DD model features of the RTC France solar cell are extracted using the suggested MLO. Table 11 lists the seven unidentified DD parameter values for different inspired techniques that yielded the best experiment outcomes. The results show that the proposed MLO outperforms corresponding approaches in terms of competitiveness. The proposed MLO achieves a desirable RMSE value of 9.82488×10^{-4}. Additionally, the table displays the electrical parameters that were generated from PV utilizing the recognized optimization methods, including RIME [53], dwarf mongoose optimizer (DMO) [72], modified RIME [53], and modified DMO [72]. Besides, the table lists the evaluated parameters of the suggested MLO, which are 1.451641269 and 2 for the ideality factor for d1 and d2, 55.43031017 Ω for shunt resistance, 0.036734969 Ω for series resistance, 0.76078101 A for photo-current, and 2.277×10^{-1} μA and 7.33063×10^{-7} μA for saturation current for d1 and d2.

Table 11. Electrical parameters obtained by the suggested MLO and LO for the DD model.

Method	DMO	RIME	MGA	MRIME	MDMO	LO	MLO
I_{Ph} (A)	0.761086003	0.760864277	0.760781079	0.760780758	0.760777046	0.760601433	0.76078101
R_{ss} (Ω)	0.036452844	0.036173672	0.03674043	0.036767981	0.03658083	0.036350742	0.036734969
R_{Sh} (Ω)	56.0407128	53.58354831	55.48544096	55.64800559	54.7047585	56.08242095	55.43031017
I_{S1} (A)	3.81141E-07	4.3113×10^{-8}	7.49347×10^{-7}	8.0438×10^{-7}	4.27843E-07	2.97805E-07	2.277E-07
η_1	1.83357911	1.827202939	2	1.999974446	1.991913976	1.49706509	1.451641269
I_{S2} (A)	2.38858E-07	3.25421×10^{-7}	2.25974×10^{-7}	2.19744×10^{-7}	2.63353×10^{-7}	3.93635E-08	7.33063E-07
η_2	1.458364626	1.482783518	1.45101678	1.448694376	1.463888853	1.427632226	2
RMSE	1.028696×10^{-3}	9.9382×10^{-4}	9.82485×10^{-4}	9.8251×10^{-4}	9.83217×10^{-4}	**9.92228E-04**	**9.82488E-04**

Figure 19(a, b) illustrates the experimental and simulated I–V and P–V curves for the DD model of the RTC France PV cell. The MLO-based results closely match the experimental data, demonstrating the method's effectiveness in predicting power and current across different voltage levels. The absolute error for power ranges from 1.97588×10^{-6} to 1.4633×10^{-3}, while the current error varies between 6.6531×10^{-9} and 6.29321×10^{-6}, as demonstrated in Figure 20(a, b).

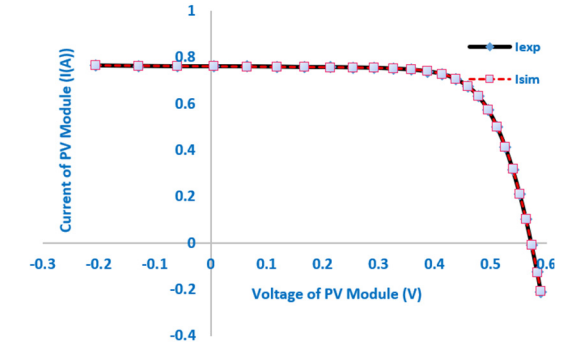

(a) I–V

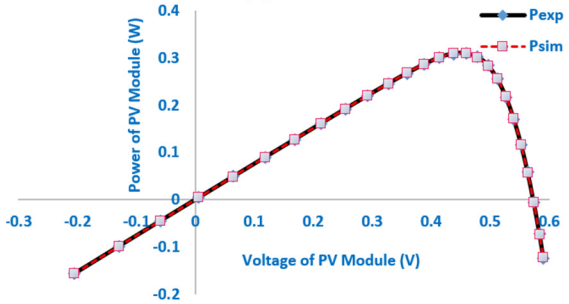

(b) P–V curve

Figure 19. Characteristic curves for the MSX-60 DD PV model, both measured and estimated.

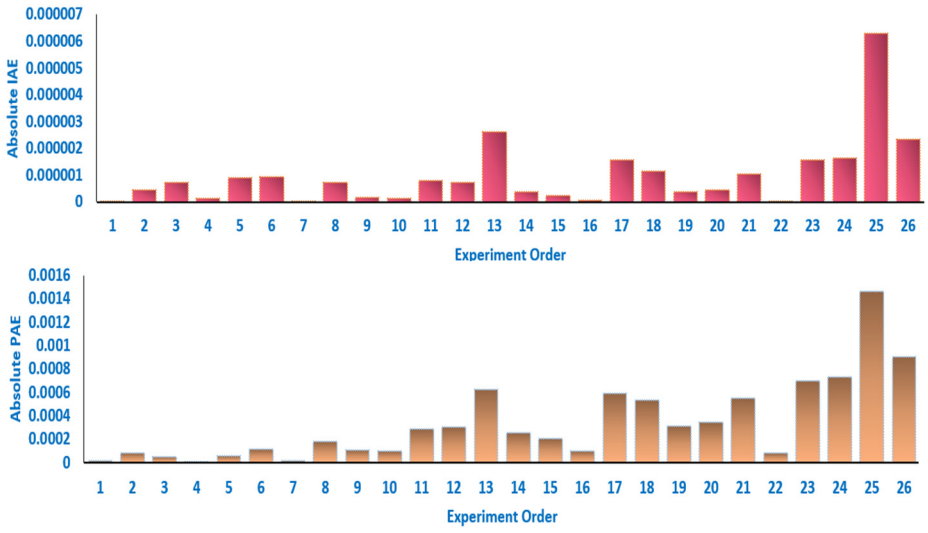

Figure 20. Absolute errors in the currents and powers between simulated and experimental values of the RTC France SD PV cell.

4.2.3. TD model

The TD model features of the RTC France solar cell are extracted using the suggested MLO. Table 12 lists the nine unidentified SD parameter values for different inspired techniques that yielded the best experiment outcomes. The results show that the proposed MLO outperforms corresponding approaches in

terms of competitiveness. This demonstrates that the proposed MLO achieves a desirable RMSE value of 9.82485×10^{-4}. Additionally, the table displays the electrical parameters that were generated from PV utilizing the recognized optimization methods, including artificial bee colony (ABC) [73], comprehensive learning PSO [74], generalized oppositional TLBO [75], hazelnut tree search (HTS) algorithm [63], cat swarm algorithm (CSA) [76], TLBO [77], growth optimizer (GO) [63], teaching–learning–based (TLABC) [78], five phases algorithm (FPA) [63], improved Kepler optimization algorithm (IKOA) [79], flower pollination optimizer (FPO) [80], energy valley optimizer (EVO) [63], sine cosine approach (SCA) [38], and improved rime metaheuristic optimization (IRMO) [81].

Based on these results, the RMSE values for the MLO method are as follows: minimum 9.82485×10^{-4}, maximum 1.00000×10^{-3}, mean 9.85554×10^{-4}, and standard deviation 2.84222×10^{-6}. Compared with other recently proposed optimization techniques, these findings demonstrate that MLO provides significantly improved accuracy and robustness in characterizing the TD model.

Table 12. Comparisons between MLO, conventional LO, and recently established competing approaches for the TD model of the RTC France PV cell.

Method	Min (RMSE)	Mean (RMSE)	Max (RMSE)	Std (RMSE)
MLO	9.82485E-04	9.85554E-04	1.00000E-03	2.84222E-06
LO	9.97454E-04	1.09032E-03	1.36650E-03	7.33831E-05
FPA [63]	1.1083E-03	1.2651E-03	1.431E-03	1.127E-04
Opposition TLBO [75]	4.43212E-03	-	-	-
TLABC [78]	1.50482E-03	-	-	-
SCA [38]	9.86863E-04	-	-	-
EVO [63]	1.083E-03	2.3850E-03	5.361E-03	1.644E-03
FPO [80]	1.934336E-03	-	-	-
TLBO [77]	1.52057E-03	-	-	-
IRMO[81]	9.86812 E-04	1.12068 E-03	1.6436 E-03	2.00229E-04
CSA [76]	1.22E-03	-	-	-
IKOA[79]	9.82490E-04	9.85769E-04	9.97427E-04	3.02730E-06
HTS [63]	1.186E-03	1.556E-03	1.988E-03	2.81E-04
ABC [73]	1.28482E-03	-	-	-
Comprehensive learning PSO [74]	1.3991E-03	-	-	-

4.2.4. Nonparametric statistical tests for compared algorithms considering the TD model

Considering the TD model of the RTC France SD PV cell, Table 13 presents the average Friedman ranks computed from repeated RMSE results across different algorithms: mantis search algorithm (MSA) [82], DMO, neural network algorithm (NNA) [82], KOA [79], IKOA [79], EVO [63], HTS [63], RMO [81], IRMO [81], GO [63], LO, and the proposed MLO. Figure 21 displays the box plot of the compared algorithms. As shown, the proposed MLO algorithm achieved the best overall rank (1.40), consistently producing the lowest RMSE values. The second-best performance is by IKOA (1.90) and GO (3.13). The original LO algorithm ranked moderately (5.87), demonstrating improvement when modified to MLO. Algorithms such as DMO, EVO, HTS, and RMO show substantially higher ranks, indicating inferior and more variable performance. Thus, the ranking results clearly demonstrate that MLO provides consistently superior optimization results.

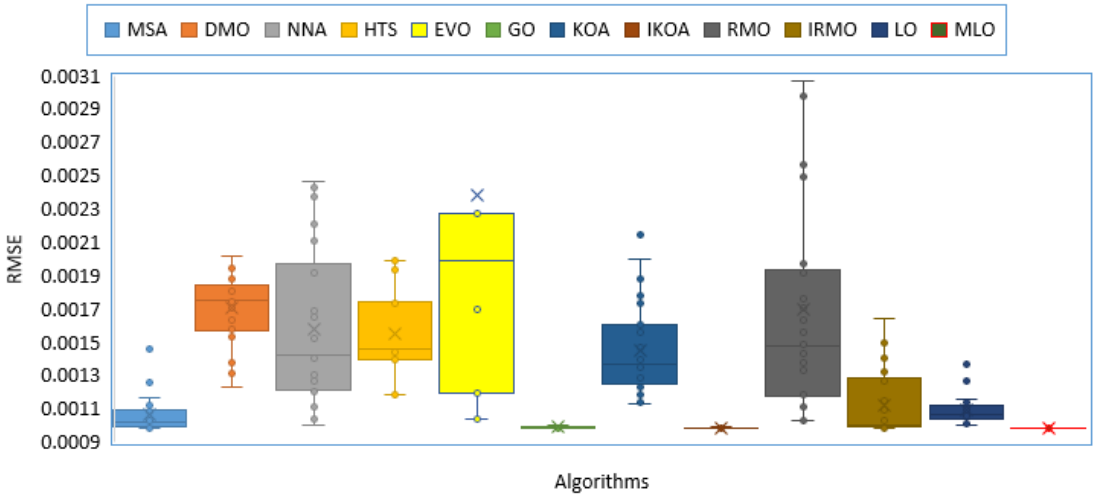

Figure 21. Box plot of the compared algorithms considering the TD model of the RTC France SD PV cell.

Table 13. Friedman statistical test.

Algorithm	Average rank	Ranking
MSA	4.87	4
DMO	10.17	12
NNA	8.60	7
HTS	9.23	10
EVO	9.63	11
GO	3.13	3
KOA	8.83	8
IKOA	1.90	2
RMO	8.97	9
IRMO	5.40	5
LO	5.87	6
MLO	1.40	1

Also, a post-hoc multiple comparisons test is implemented between each pair of algorithms, as shown in Table 14. Several comparisons involving MLO vs. other algorithms produced p-values < 0.05, confirming significant performance improvements. The comparison between MLO and GO/IKOA did not yield statistical significance ($p = 1$); while MLO ranks higher, their result distributions were close enough to not be statistically different in this post-hoc test. However, the pairwise Wilcoxon test (Table 15) confirms significance where Dunn did not.

Table 14. Post-hoc multiple comparisons statistical test.

Algorithm 1	Algorithm 2	Lower_CI	Mean_Diff	Upper_CI	p_value
MSA	DMO	−8.4288	−5.3	−2.1712	0.00003
MSA	NNA	−6.8622	−3.7333	−0.6045	0.004
MSA	HTS	−7.4955	−4.3667	−1.2378	0.0002
MSA	EVO	−7.8955	−4.7667	−1.6378	0.00001
MSA	GO	−1.3955	1.7333	4.8622	0.986
MSA	KOA	−7.0955	−3.9667	−0.8378	0.0013
MSA	IKOA	−0.1622	2.9667	6.0955	0.0907
MSA	RMO	−7.2288	−4.1	−0.9712	0.0007
MSA	IRMO	−3.6622	−0.5333	2.5955	1
MSA	LO	−4.1288	−1	2.1288	1
MSA	MLO	0.3378	3.4667	6.5955	0.0129
DMO	NNA	−1.5622	1.5667	4.6955	0.9983
DMO	HTS	−2.1955	0.9333	4.0622	1
DMO	EVO	−2.5955	0.5333	3.6622	1
DMO	GO	3.9045	7.0333	10.1622	0.000002
DMO	KOA	−1.7955	1.3333	4.4622	1
DMO	IKOA	5.1378	8.2667	11.3955	0.000012
DMO	RMO	−1.9288	1.2	4.3288	1
DMO	IRMO	1.6378	4.7667	7.8955	0.0000059
DMO	LO	1.1712	4.3	7.4288	0.0003
DMO	MLO	5.6378	8.7667	11.8955	0.000015
NNA	HTS	−3.7622	−0.6333	2.4955	1
NNA	EVO	−4.1622	−1.0333	2.0955	1
NNA	GO	2.3378	5.4667	8.5955	0.000022
NNA	KOA	−3.3622	−0.2333	2.8955	1
NNA	IKOA	3.5712	6.7	9.8288	0.00001
NNA	RMO	−3.4955	−0.3667	2.7622	1
NNA	IRMO	0.0712	3.2	6.3288	0.038
NNA	LO	−0.3955	2.7333	5.8622	0.1973
NNA	MLO	4.0712	7.2	10.3288	0.0000001
HTS	EVO	−3.5288	−0.4	2.7288	1
HTS	GO	2.9712	6.1	9.2288	0.000003
HTS	KOA	−2.7288	0.4	3.5288	1
HTS	IKOA	4.2045	7.3333	10.4622	0.00002
HTS	RMO	−2.8622	0.2667	3.3955	1
HTS	IRMO	0.7045	3.8333	6.9622	0.0025
HTS	LO	0.2378	3.3667	6.4955	0.0195
HTS	MLO	4.7045	7.8333	10.9622	0.000005
EVO	GO	3.3712	6.5	9.6288	0.000006
EVO	KOA	−2.3288	0.8	3.9288	1

Continued on next page

Algorithm 1	Algorithm 2	Lower_CI	Mean_Diff	Upper_CI	p_value
EVO	IKOA	4.6045	7.7333	10.8622	0.000008
EVO	RMO	−2.4622	0.6667	3.7955	1
EVO	IRMO	1.1045	4.2333	7.3622	0.0004
EVO	LO	0.6378	3.7667	6.8955	0.0034
EVO	MLO	5.1045	8.2333	11.3622	0.000023
GO	KOA	−8.8288	−5.7	−2.5712	0.000027
GO	IKOA	−1.8955	1.2333	4.3622	1
GO	RMO	−8.9622	−5.8333	−2.7045	0.0000075
GO	IRMO	−5.3955	−2.2667	0.8622	0.6287
GO	LO	−5.8622	−2.7333	0.3955	0.1973
GO	MLO	−1.3955	1.7333	4.8622	0.986
KOA	IKOA	3.8045	6.9333	10.0622	0.0000025
KOA	RMO	−3.2622	−0.1333	2.9955	1
KOA	IRMO	0.3045	3.4333	6.5622	0.0148
KOA	LO	−0.1622	2.9667	6.0955	0.0907
KOA	MLO	4.3045	7.4333	10.5622	0.0000056
IKOA	RMO	−10.1955	−7.0667	−3.9378	0.000009
IKOA	IRMO	−6.6288	−3.5	−0.3712	0.0112
IKOA	LO	−7.0955	−3.9667	−0.8378	0.0013
IKOA	MLO	−2.6288	0.5	3.6288	1
RMO	IRMO	0.4378	3.5667	6.6955	0.0084
RMO	LO	−0.0288	3.1	6.2288	0.0557
RMO	MLO	4.4378	7.5667	10.6955	0.0000023
IRMO	LO	−3.5955	−0.4667	2.6622	1
IRMO	MLO	0.8712	4	7.1288	0.0011
LO	MLO	1.3378	4.4667	7.5955	0.0001

Furthermore, the Wilcoxon signed-rank test was employed to evaluate the run-to-run performance consistency between the algorithms, as summarized in Table 15. The results clearly demonstrate that the proposed MLO algorithm exhibits significantly superior performance when compared with all other competing methods, including LO, with p-values less than 0.05 in all direct pairwise comparisons. This confirms that the improvement offered by MLO is not only reflected in average accuracy but is also consistent and repeatable across multiple independent runs. It is noteworthy that the comparison between MLO and IKOA yielded a p-value of 0.0166, which, although still below the 0.05 significance threshold, indicates a comparatively smaller but still statistically significant performance advantage for MLO. This suggests that while IKOA is among the stronger baseline competitors, the proposed modifications implemented in MLO provide a more stable and robust optimization behavior overall.

Table 15. Pairwise Wilcoxon signed-rank statistical test.

MLO vs. algorithm	p-value
MLO vs. MSA	1.9209E-06
MLO vs. DMO	1.7344E-06
MLO vs. NNA	1.7344E-06
MLO vs. HTS	1.7344E-06
MLO vs. EVO	1.7300E-06
MLO vs. GO	4.2857E-06
MLO vs. KOA	1.7344E-06
MLO vs. IKOA	1.6566E-02
MLO vs. RMO	1.7344E-06
MLO vs. IRMO	1.7344E-06
MLO vs. LO	1.7344E-06

4.2.5. Electrical characteristics of the RTC France solar cell considering the TD model

Figure 22(a, b) presents the experimental and simulated I–V and P–V curves for the TD model of the RTC France PV cell. The results generated using the proposed MLO approach show a strong correlation with experimental measurements, confirming its effectiveness in predicting power and current across various voltage levels. The absolute error for power ranges from 1.86255×10^{-6} to 1.4881×10^{-3}, while the current error varies between 2.82332×10^{-10} and 6.50807×10^{-6}, as demonstrated in Figure 23(a, b).

Figure 24 illustrates the convergence graphs of the proposed MLO and the conventional LO for the SD, DD, and TD PV model of the RTC France PV cell. Figure 24(a–c) shows that the proposed MLO from the beginning of the iterative journey is associated with significant progress. This is due to an improvement in the exploration capability made possible by the MLO approach. The improvement starts at iteration 200 for all three models with the best converging attributes.

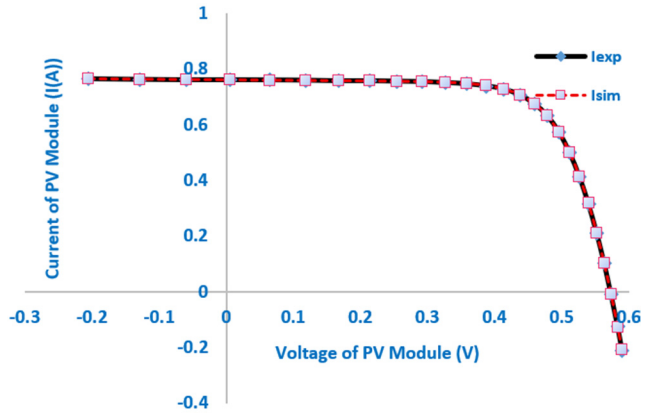

(a) I–V

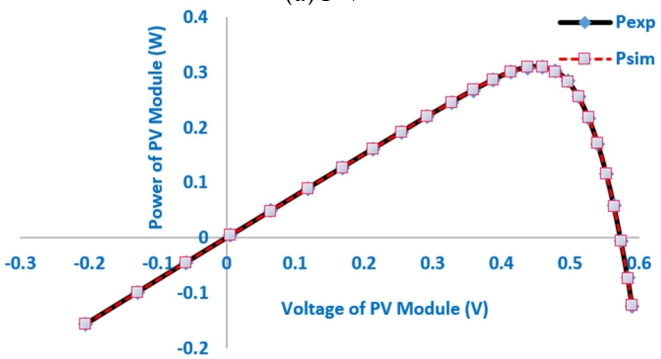

(b) P–V curve

Figure 22. Characteristic curves for the MSX-60 TD PV model, both measured and estimated.

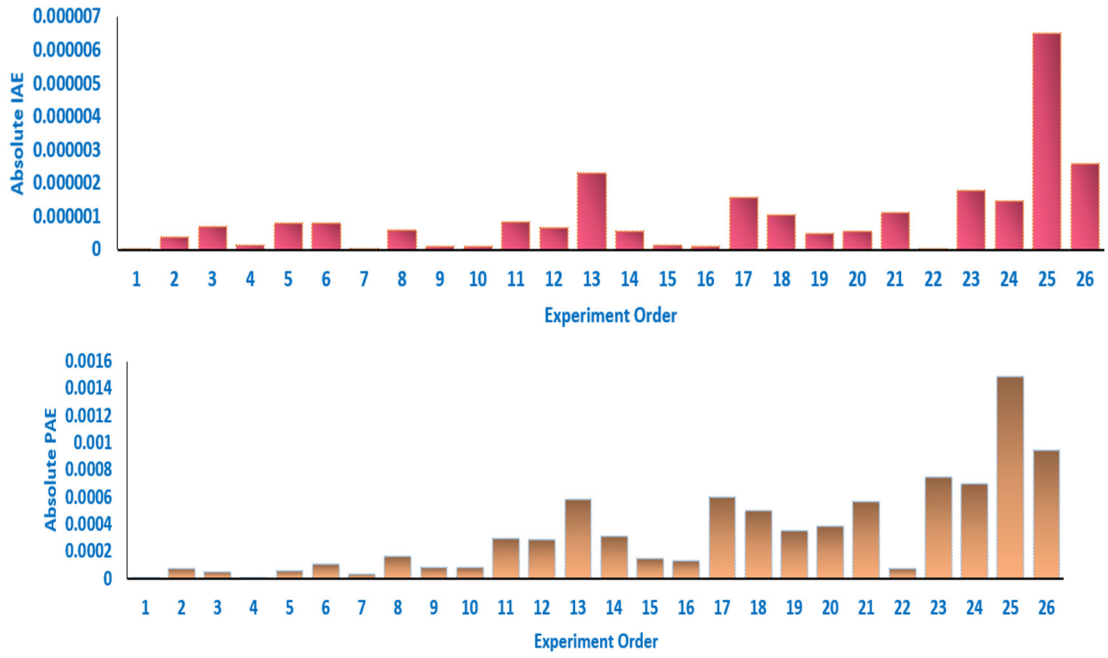

Figure 23. Absolute errors in the currents and powers between simulated and experimental values of the RTC France SD PV cell.

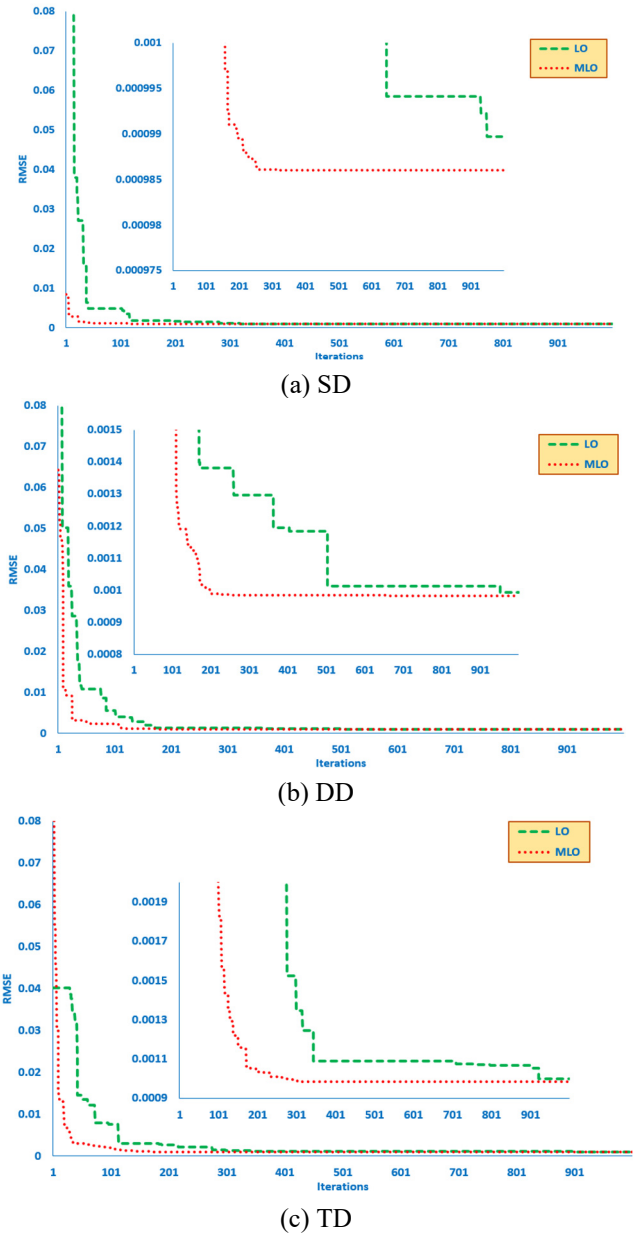

Figure 24. Convergence graphs of the proposed MLO and the conventional LO for the SD, DD, and TD PV model of RTC France PV cell.

4.2.6. Ablation study and sensitivity analysis of the RTC France solar cell considering the TD model

This study proposes two primary interrelated changes (MBLSS/DMLSS). To show that each modification matters, an ablation study is included in this section by implementing (i) standard LO, (ii) LO + MBLSS only, (iii) LO + DMLSS only, and (iv) full MLO, and comparing the different indicators of the RMSE to demonstrate the contribution of each component. As shown in Table 16, the full MLO achieves the best performance across all evaluation indicators, with a minimum RMSE of 0.00098249, mean RMSE of 0.00098555, maximum RMSE of 0.00100000, and standard deviation of 2.8422×10^{-6},

indicating highly stable convergence. Introducing MBLSS alone improves stability significantly compared to standard LO, reducing the standard deviation from 7.338×10^{-5} to 7.097×10^{-6}, and lowering the mean RMSE from 0.0010903 to 0.0009886. Meanwhile, DMLSS alone enhances global search ability, but yields slightly higher variation (Std = 3.0584×10^{-5}) and mean RMSE (0.00104518) than MBLSS. The best performance is obtained when both strategies are combined, demonstrating a synergistic effect in improving accuracy and robustness.

Table 16. Ablation study of the RTC France solar cell considering the TD model.

	LO	LO+MBLSS	LO+DMLSS	MLO (proposed)
Min (RMSE)	0.0009975	0.0009841	0.00101468	0.00098249
Mean (RMSE)	0.0010903	0.0009886	0.00104518	0.00098555
Max (RMSE)	0.0013665	0.0010078	0.00109726	0.001
Std (RMSE)	7.338E-05	7.097E-06	3.0584E-05	2.8422E-06

To further evaluate the robustness of the MLO algorithm, a sensitivity analysis was conducted on the imitation probability P_m and the distance coefficient γ. Tables 17 and 18 report the minimum RMSE and standard deviation obtained across combinations of $P_m \in [0,1]$ and $\gamma \in [0,1]$. From Table 17, the lowest minimum RMSE values are observed when $P_m = 0.5$ and $\gamma = 0.5$ (minimum RMSE = 0.00098458), and when $P_m = 0.75$ and $\gamma = 0.25$ (minimum RMSE = 0.00098560). Similarly, the standard deviations (Table 18) show their smallest values at $P_m = 0.5, \gamma = 0.5$ with Std = 1.3972×10^{-6}, and $P_m = 0.75, \gamma = 0.25$ with Std = 9.1676×10^{-7} demonstrating highly stable output. In contrast, extreme values of $P_m = 0$ or $P_m = 1$, combined with high γ, lead to degraded performance (e.g., RMSE increases to 0.00273855 when $P_m = 0, \gamma = 0.75$). These results indicate that moderate parameter values (i.e., $P_m = 0.5$–0.75, $\gamma = 0.25$–0.50) provide the best balance between learning influence and search diversification.

Table 17. Sensitivity analysis of the proposed MLO considering the minimum obtained RMSE.

Parameters	$\gamma = 0$	$\gamma = 0.25$	$\gamma = 0.5$	$\gamma = 0.75$	$\gamma = 1$
Pm = 0	0.00107059	0.00109641	0.00104518	0.00273855	0.00259594
Pm = 0.25	0.00098856	0.00099008	0.00110661	0.00101240	0.00102182
Pm = 0.5	0.00100621	0.00102290	**0.000984583**	0.000984591	0.00105350
Pm = 0.75	0.00100518	0.00098560	0.00098700	0.00105285	0.00098632
Pm = 1	0.00142479	0.00140869	0.00106247	0.00111331	0.00107447

Table 18. Sensitivity analysis of the proposed MLO considering the obtained standard deviations of the RMSE.

Parameters	$\gamma = 0$	$\gamma = 0.25$	$\gamma = 0.5$	$\gamma = 0.75$	$\gamma = 1$
Pm = 0	4.1338E-05	8.1261E-05	3.0584E-05	1.3513E-03	9.8881E-04
Pm = 0.25	7.0972E-06	1.0163E-05	2.6315E-04	5.0570E-05	1.0443E-04
Pm = 0.5	3.7155E-05	1.1474E-04	**1.3972E-06**	1.0773E-05	1.5175E-04
Pm = 0.75	3.9329E-05	9.1676E-07	2.1298E-06	1.5399E-04	3.3501E-06
Pm = 1	6.0170E-04	6.0474E-04	1.7517E-04	1.7842E-04	2.0349E-04

4.3. Application to the shell S75 PV module

In this part, the MLO and LO application is extended to the Shell S75, and evaluated under an irradiance of 1000 W/m², a cell temperature of 25 °C, and an air mass of AM 1.5. Its electrical characteristics include an open-circuit voltage of 21.60 V and a short-circuit current of 4.70 A. At the maximum power operating point, the module delivers 17.60 V and 4.26 A, resulting in a rated maximum output power of 75 W. The temperature coefficients are 2 mA/°C for the short-circuit current and −76 mV/°C for the open-circuit voltage, indicating increasing current and decreasing voltage with rising temperature [83].

Figures 25 and 26 illustrate the I–V and P–V curves under varying irradiance and temperature levels, respectively, showing that MLO accurately reproduces the electrical characteristics across different operating conditions.

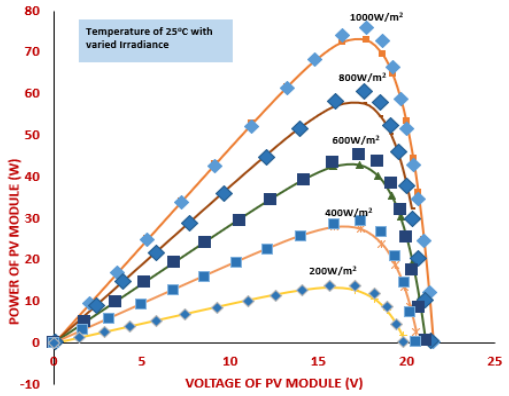

(a) I–V

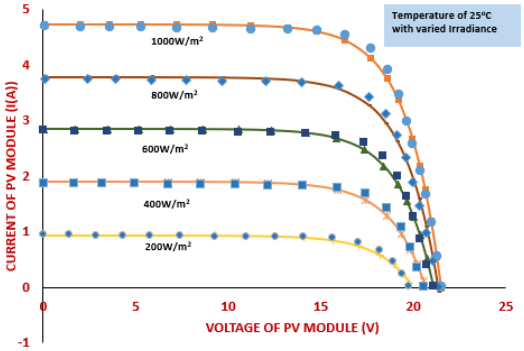

(b) P–V

Figure 25. Electrical characteristics under different irradiance levels and a temperature of 25 °C of the S75 PV module.

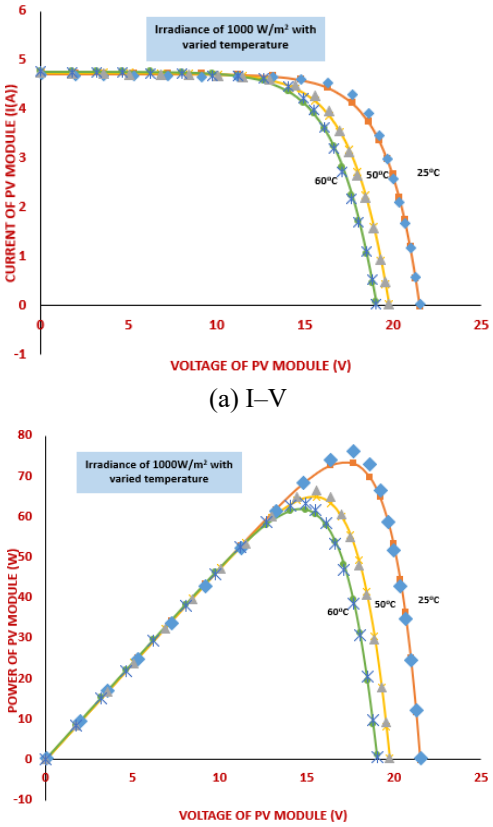

(a) I–V

(b) P–V

Figure 26. Electrical characteristics under different temperatures and 1000 W/m^2 irradiance of the S75 PV module.

As shown in Table 19, under varying irradiance (200–1000 W/m²), the proposed MLO consistently achieves lower RMSE values compared to LO. At 800 W/m², MLO achieves a minimum RMSE of 0.086708, whereas LO yields 0.086794–0.087026 with a standard deviation of 7.75 × 10^{-5}, demonstrating that LO suffers from higher fluctuation. Notably, MLO maintains near-zero variance across all irradiance levels (Std in the range of ~10^{-17}), confirming its high stability and repeatability.

Table 19. LO versus MLO under different irradiance levels and a temperature of 25 °C of the S75 PV module.

	Irradiance	Applied technique	Min	Max	Average	Std
Temperature of 25 °C	200	LO	0.034502	0.034721	0.034937	0.000155
		MLO	0.034393	0.034393	0.034393	3.27E-18
	400	LO	0.069784	0.069957	0.070476	0.000238
		MLO	0.069599	0.069599	0.069599	1.31E-17
	600	LO	0.079938	0.080096	0.080541	0.000176
		MLO	0.079817	0.079817	0.079817	6.54E-18
	800	LO	0.086794	0.08688	0.087026	7.75E-05
		MLO	0.086708	0.086708	0.086708	1.46E-17
	1000	LO	0.074198	0.074353	0.074682	0.000137
		MLO	0.074144	0.074144	0.074144	9.25E-18

Table 20 further evaluates performance under temperature variations (25–60 °C) at 1000 W/m². At 25 °C, MLO again outperforms LO, achieving a stable RMSE of 0.074144 with a negligible standard deviation of 9.25×10^{-18}, compared to LO's 0.074198–0.0746816 and Std of 1.37×10^{-4}. At elevated temperatures (e.g., 60 °C), both methods experience RMSE increases due to intensified thermal influence on diode currents and shunt resistance, but MLO still provides a lower minimum RMSE (0.053744) than LO (0.0539443). However, MLO exhibits a higher spread at high temperature (Std 3.08×10^{-3}), indicating that extreme thermal conditions introduce stronger nonlinear effects.

These results confirm that MLO delivers higher accuracy and superior stability across a wide range of operating conditions, while maintaining robustness even when the PV model becomes more sensitive to temperature.

Table 20. Sensitivity analysis of the proposed MLO under different temperatures and 1000 W/m^2 irradiance of the S75 PV module.

	Temperature	Applied technique	Min	Max	Average	Std
Irradiance of 1000 W/m^2	25	LO	0.074198	0.0743529	0.0746816	1.3672E-04
		MLO	0.0741441	0.0741441	0.0741441	9.2519E-18
	50	LO	0.048509	0.0489207	0.0496301	3.5887E-04
		MLO	0.048171	0.0492322	0.0587022	3.3275E-03
	60	LO	0.0539443	0.0545159	0.0557607	5.4032E-04
		MLO	0.0537439	0.0548686	0.0635511	3.0765E-03

5. Conclusions

This work presented a modified lyrebird optimization (MLO) algorithm for the accurate extraction of photovoltaic model parameters, addressing the limitations of conventional approaches. The proposed MLO enhanced the original lyrebird optimization (LO) framework by introducing two major improvements: a memory-based learn search strategy (MBLSS) to strengthen exploration and a diversity maintenance learn search strategy (DMLSS) to improve exploitation. Furthermore, the effectiveness of the proposed MLO was validated through extensive experiments on two well-known PV systems, the RTC France solar cell and the Solarex MSX-60 module, under SD, DD, and TD models. Comparative analyses against the conventional LO and several recent metaheuristic and analytical techniques revealed that MLO consistently achieved lower RMSE, faster convergence, and higher stability. Additional validation on the Shell S75 module demonstrated that MLO remains effective under fluctuating irradiance and temperature conditions, achieving lower minimum RMSE values and significantly reduced variance compared to LO. Even at high temperature operating ranges where nonlinear effects intensify, MLO preserved superior accuracy, indicating its suitability for real-world PV modeling, performance estimation, and control applications. Statistical evaluations of 50 independent runs confirmed the reliability and robustness of the MLO. Additionally, the strong agreement between experimental and simulated I–V and P–V curves demonstrated the accuracy of the extracted parameters.

Under an equal computational budget of 100,000 function evaluations, the MLO yielded superior performance with an average runtime of ~57.7 s, which is only moderately higher than the ~38.6 s of LO, but delivered significantly improved precision and robustness. The ablation study confirmed that both the MBLSS and DMLSS contribute meaningfully to performance. The integrated MBLSS

enhanced convergence stability (Std reduced from 7.338×10^{-5} to 7.097×10^{-6}), whereas the DMLSS improved global exploration. Their combination in the full MLO configuration achieved the best results (minimum RMSE = 0.00098249 and Std = 2.8422×10^{-6}). Additionally, the sensitivity analysis on the imitation probability and distance coefficient revealed optimal performance for moderate parameter values $P_m = 0.5 \sim 0.75$ and $\gamma = 0.25 \sim 0.50$, demonstrating that balanced learning influence and diversity control are crucial for reliable convergence. These findings declare that the proposed MLO is a reliable tool for PV parameter identification. By providing accurate and stable parameter estimation, MLO contributes to improved modeling, performance evaluation, and control of PV systems, which are crucial for efficient energy forecasting and grid integration. Future work may extend MLO to real-time monitoring, incorporate environmental variability, and hybridize with other techniques.

Despite the strong results, some limitations remain. First, validation is required for broader PV technologies and real dynamic field environments. Second, while the bounds used for diode ideality factors ensured physical plausibility, occasional convergence to the limits suggests potential parameter identifiability issues under certain datasets. Future work will therefore include: (i) testing the MLO on additional PV technologies (monocrystalline, polycrystalline, and thin-film) and commercial modules such as PWP201, STM6, SM55, S75, and ST40, (ii) extending validation to partial shading and dynamic irradiance/temperature profiles, (iii) integrating adaptive or self-tuning mechanisms to eliminate manual hyperparameter selection, and (iv) applying the proposed MLO to real-time MPPT and energy-management systems.

Author contributions

Sultan Hakmi: Resources; Methodology; Project administration; Supervision; Roles and Writing original draft. **Ghareeb Moustafa**: Data curation; Formal analysis; Writing—review and editing. **Hashim Alnami**.: Formal analysis; Methodology; Project administration; Roles and Writing original draft. **Badr M Al Faiya**: Data curation; Formal analysis; Validation; Roles/Writing original draft. **Ahmed Ginidi**: Validation; Methodology; Software; Project administration; Writing—review and editing.

Acknowledgments

The authors gratefully acknowledge the funding of the Deanship of Graduate Studies and Scientific Research, Jazan University, Saudi Arabia, through Project number: (JU- 20250228 - DGSSR-RP-2025).

Use of Generative-AI tools declaration

The authors declare they have not used Artificial Intelligence (AI) tools in the creation of this article.

Data availability

Code is available upon request.

Conflict of interest

The authors declare no competing interests.

References

1. H. Abdulla, A. Sleptchenko, A. Nayfeh, Photovoltaic systems operation and maintenance: A review and future directions, *Renewable Sustainable Energy Rev.*, **195** (2024), 114342. https://doi.org/10.1016/j.rser.2024.114342
2. M. H. Alqahtani, A. M. Shaheen, M. A. Atiea, A meteorology-free wind power forecasting using a hybrid physics-aware, SCADA-only ensemble residual learning, *Results Eng.*, **28** (2025), 107285. https://doi.org/10.1016/j.rineng.2025.107285
3. A. Aslam, N. Ahmed, S. A. Qureshi, M. Assadi, N. Ahmed, Advances in Solar PV Systems; A Comprehensive Review of PV Performance, Influencing Factors, and Mitigation Techniques, *Energies*, **15** (2022), 75952022. https://doi.org/10.3390/en15207595
4. A. Massi Pavan, S. Vergura, A. Mellit, V. Lughi, Explicit empirical model for photovoltaic devices. Experimental validation, *Sol. Energy*, **155** (2017), 647–653. https://doi.org/10.1016/j.solener.2017.07.002
5. V. J. Chin, Z. Salam, K. Ishaque, An accurate modelling of the two-diode model of PV module using a hybrid solution based on differential evolution, *Energy Convers. Manag.*, **124** (2016), 42–50. https://doi.org/10.1016/j.enconman.2016.06.076
6. F. J. Toledo, J. M. Blanes, Analytical and quasi-explicit four arbitrary point method for extraction of solar cell single-diode model parameters, *Renew. Energy*, **92** (2016), 346–356. https://doi.org/10.1016/j.renene.2016.02.012
7. J. Cubas, S. Pindado, M. Victoria, On the analytical approach for modeling photovoltaic systems behavior, *J. Power Sources*, **247** (2014), 467–474. https://doi.org/10.1016/j.jpowsour.2013.09.008
8. A. Jain, S. Sharma, A. Kapoor, Solar cell array parameters using Lambert W-function, *Sol. Energy Mater. Sol. Cells*, **90** (2006), 25–31. https://doi.org/10.1016/j.solmat.2005.01.007
9. A. Ortiz-Conde, F. J. García Sánchez, J. Muci, New method to extract the model parameters of solar cells from the explicit analytic solutions of their illuminated I–V characteristics, *Sol. Energy Mater. Sol. Cells*, **90** (2006), 352–361. https://doi.org/10.1016/j.solmat.2005.04.023
10. M. Bencherif, N. Brahmi, Solar cell parameter identification using the three main points of the current-voltage characteristic, *Int. J. Ambient Energy*, **43** (2020), 3064–3084. https://doi.org/10.1080/01430750.2020.1789739
11. S. Li, W. Gong, Q. Gu, A comprehensive survey on meta-heuristic algorithms for parameter extraction of photovoltaic models, *Renew. Sustain. Energy Rev.*, **141** (2021), 110828. https://doi.org/10.1016/j.rser.2021.110828
12. T. Easwarakhanthan, J. Bottin, I. Bouhouch, C. Boutrit, Nonlinear Minimization Algorithm for Determining the Solar Cell Parameters with Microcomputers, *Int. J. Sol. Energy*, **4** (1986), 1–12. https://doi.org/10.1080/01425918608909835
13. S. Liu, R. A. Dougal, Dynamic multiphysics model for solar array, *IEEE Trans. Energy Convers.*, **17** (2002), 285–294. https://doi.org/10.1109/TEC.2002.1009482

14. M. Zagrouba, A. Sellami, M. Bouaïcha, M. Ksouri, Identification of PV solar cells and modules parameters using the genetic algorithms: Application to maximum power extraction, *Sol. Energy*, **84** (2010), 860–866. https://doi.org/10.1016/j.solener.2010.02.012
15. I. Choulli, M. Elyaqouti, E. Arjdal, D. Ben Hmamou, D. Saadaoui, S. Lidaighbi, et al., DIWJAYA: JAYA driven by individual weights for enhanced photovoltaic model parameter estimation, *Energy Convers. Manag.*, **305** (2024), 118258. https://doi.org/10.1016/j.enconman.2024.118258
16. X. Ru, Parameter extraction of photovoltaic model based on butterfly optimization algorithm with chaos learning strategy, *Sol. Energy*, **269** (2024), 112353. https://doi.org/10.1016/j.solener.2024.112353
17. D. Saadaoui, M. Elyaqouti, K. Assalaou, D. Ben Hmamou, S. Lidaighbi, E. Arjdal, et al., A hybrid optimization algorithm to identify unknown parameters of photovoltaic models under varying operating conditions, *Eng. Appl. Artif. Intell.*, **133** (2024), 108544. https://doi.org/10.1016/j.engappai.2024.108544
18. S. Z. Almutairi, A. M. Shaheen, A novel kangaroo escape optimizer for parameter estimation of solar photovoltaic cells/modules via one, two and three-diode equivalent circuit modeling, *Sci. Rep.*, **15** (2025), 32669. https://doi.org/10.1038/s41598-025-19917-4
19. I. Abazine, M. Elyaqouti, E. Arjdal, D. Saadaoui, D. Ben Hmamou, A. Elhammoudy, et al., Accurate parameter extraction for photovoltaic systems using an improved and stable hybrid Analytical-NRBO algorithm, *Int. J. Hydrogen Energy*, **139** (2025), 564–593. https://doi.org/10.1016/j.ijhydene.2025.05.208
20. S. Yu, A. A. Heidari, G. Liang, C. Chen, H. Chen, Q. Shao, Solar photovoltaic model parameter estimation based on orthogonally-adapted gradient-based optimization, *Optik*, **252** (2022), 168513. https://doi.org/10.1016/j.ijleo.2021.168513
21. I. H. Smaili, G. Moustafa, D. R. Almalawi, A. Ginidi, A. M. Shaheen, H. S. E. Mansour, Enhanced Artificial Rabbits Algorithm Integrating Equilibrium Pool to Support PV Power Estimation via Module Parameter Identification, *Int. J. Energy Res.*, **2024** (2024), 8913560. https://doi.org/10.1155/2024/8913560
22. A. E. Ramadan, S. Kamel, T. Khurshaid, S. R. Oh, S. B. Rhee, Parameter Extraction of Three Diode Solar Photovoltaic Model Using Improved Grey Wolf Optimizer, *Sustainability*, **13** (2021), 6963. https://doi.org/10.3390/su13126963
23. M. A. Khelifa, B. Lekouaghet, and A. Boukabou, Symmetric chaotic gradient-based optimizer algorithm for efficient estimation of PV parameters, *Optik (Stuttg).*, **259** (2022), 168873. https://doi.org/10.1016/j.ijleo.2022.168873
24. P. J. Gnetchejo, S. N. Essiane, P. Ele, R. Wamkeue, D. M. Wapet, S. P. Ngoffe, Enhanced Vibrating Particles System Algorithm for Parameters Estimation of Photovoltaic System, *J. Power Energy Eng.*, **07** (2019), 1. https://doi.org/10.4236/jpee.2019.78001.
25. A. A. Z. Diab, H. M. Sultan, R. Aljendy, A. S. Al-Sumaiti, M. Shoyama, Z. M. Ali, Tree Growth Based Optimization Algorithm for Parameter Extraction of Different Models of Photovoltaic Cells and Modules, *IEEE Access*, **8** (2020), 119668–119687. https://doi.org/10.1109/ACCESS.2020.3005236
26. A. M. Shaheen, A. M. Elsayed, A. R. Ginidi, R. A. El-Sehiemy, E. Elattar, Enhanced social network search algorithm with powerful exploitation strategy for PV parameters estimation, *Energy Sci. Eng.*, **10** (2022), 1398–1417. https://doi.org/10.1002/ESE3.1109

27. C. Kumar, D. Magdalin Mary, A novel chaotic-driven Tuna Swarm Optimizer with Newton-Raphson method for parameter identification of three-diode equivalent circuit model of solar photovoltaic cells/modules, *Optik*, **264** (2022), 169379. https://doi.org/10.1016/j.ijleo.2022.169379
28. A. Abbassi, R. Ben Mehrez, Y. Bensalem, R. Abbassi, M. Kchaou, M. Jemli, et al., Improved Arithmetic Optimization Algorithm for Parameters Extraction of Photovoltaic Solar Cell Single-Diode Model, *Arab. J. Sci. Eng.*, **47** (2022), 10435–10451. https://doi.org/10.1007/s13369-022-06605-y.
29. D. Izci, S. Ekinci, A. G. Hussien, Efficient parameter extraction of photovoltaic models with a novel enhanced prairie dog optimization algorithm, *Sci. Rep.*, **14** (2024), 1–20, Apr., doi: https://doi.org/10.1038/s41598-024-58503-y
30. D. T. Cotfas, A. M. Deaconu, P. A. Cotfas, Hybrid successive discretisation algorithm used to calculate parameters of the photovoltaic cells and panels for existing datasets, *IET Renew. Power Gener.*, **15** (2021), 3661–3687. https://doi.org/10.1049/RPG2.12262
31. A. R. Ginidi, A. M. Shaheen, R. A. El-Sehiemy, H. M. Hasanien, A. Al-Durra, Estimation of electrical parameters of photovoltaic panels using heap-based algorithm, *IET Renew. Power Gener.*, **16** (2022), 2292–2312. https://doi.org/10.1049/rpg2.12523
32. P. J. Gnetchejo, S. Ndjakomo Essiane, P. Ele, R. Wamkeue, D. Mbadjoun Wapet, S. Perabi Ngoffe, Important notes on parameter estimation of solar photovoltaic cell, *Energy Convers. Manag.*, **197 (**2019**)**, 111870. https://doi.org/10.1016/J.ENCONMAN.2019.111870
33. R. Abbassi, S. Saidi, S. Urooj, B. N. Alhasnawi, M. A. Alawad, M. Premkumar, An Accurate Metaheuristic Mountain Gazelle Optimizer for Parameter Estimation of Single- and Double-Diode Photovoltaic Cell Models, *Mathematics*, **11** (2023), 4565. https://doi.org/10.3390/math11224565
34. H. Rezk, M. A. Abdelkareem, Optimal parameter identification of triple diode model for solar photovoltaic panel and cells, *Energy Rep.*, **8** (2022), 1179–1188. https://doi.org/10.1016/j.egyr.2021.11.179
35. H. Chen, S. Jiao, M. Wang, A. A. Heidari, X. Zhao, Parameters identification of photovoltaic cells and modules using diversification-enriched Harris hawks optimization with chaotic drifts, *J. Clean. Prod.*, **244** (2020), 118778. https://doi.org/10.1016/j.jclepro.2019.118778
36. Z. Wu, D. Yu, X. Kang, Parameter identification of photovoltaic cell model based on improved ant lion optimizer, *Energy Convers. Manag.*, **151** (2017), 107–115. https://doi.org/10.1016/J.ENCONMAN.2017.08.088
37. H. M. Ridha, A. A. Heidari, M. Wang, H. Chen, Boosted mutation-based Harris hawks optimizer for parameters identification of single-diode solar cell models, *Energy Convers. Manag.*, **209** (2020), 112660. https://doi.org/10.1016/J.ENCONMAN.2020.112660
38. H. Chen, S. Jiao, A. A. Heidari, M. Wang, X. Chen, X. Zhao, An opposition-based sine cosine approach with local search for parameter estimation of photovoltaic models, *Energy Convers. Manag.*, **195** (2019), 927–942. https://doi.org/10.1016/J.ENCONMAN.2019.05.057
39. Y. Liu, G. Chong, A. Asghar Heidari, H. Chen, G. Liang, X. Ye, et al., Horizontal and vertical crossover of Harris hawk optimizer with Nelder-Mead simplex for parameter estimation of photovoltaic models, *Energy Convers. Manag.*, **223** (2020), 113211. https://doi.org/10.1016/J.ENCONMAN.2020.113211

40. H. Zhang, A. A. Heidari, M. Wang, L. Zhang, H. Chen, C. Li, Orthogonal Nelder-Mead moth flame method for parameters identification of photovoltaic modules, *Energy Convers. Manag.*, **211** (2020), 112764. https://doi.org/10.1016/J.ENCONMAN.2020.112764
41. M. Qaraad, S. Amjad, N. K. Hussein, M. A. Farag, S. Mirjalili, M. A. Elhosseini, Quadratic interpolation and a new local search approach to improve particle swarm optimization: Solar photovoltaic parameter estimation, *Expert Syst. Appl.*, **236** (2024), 121417. https://doi.org/10.1016/j.eswa.2023.121417
42. P. J. Gnetchejo, S. Ndjakomo Essiane, A. Dadjé, P. Ele, A combination of Newton-Raphson method and heuristics algorithms for parameter estimation in photovoltaic modules, *Heliyon*, **7** (2021), e06673. https://doi.org/10.1016/J.HELIYON.2021.E06673
43. M. Qaraad, S. Amjad, N. K. Hussein, M. Badawy, S. Mirjalili, M. A. Elhosseini, Photovoltaic parameter estimation using improved moth flame algorithms with local escape operators, *Comput. Electr. Eng.*, **106** (2023), 108603. https://doi.org/10.1016/j.compeleceng.2023.108603
44. D. Maden, E. Çelik, E. H. Houssein, G. Sharma, Squirrel search algorithm applied to effective estimation of solar PV model parameters: a real-world practice, *Neural Comput. Appl.*, **35** (2023), 13529–13546. https://doi.org/10.1007/s00521-023-08451-x
45. H. G. G. Nunes, J. A. N. Pombo, S. J. P. S. Mariano, M. R. A. Calado, J. A. M. Felippe de Souza, A new high performance method for determining the parameters of PV cells and modules based on guaranteed convergence particle swarm optimization, *Appl. Energy*, **211** (2018), 774–791. https://doi.org/10.1016/J.APENERGY.2017.11.078
46. A. M. Shaheen, R. A. El-Seheimy, G. Xiong, E. Elattar, A. R. Ginidi, Parameter identification of solar photovoltaic cell and module models via supply demand optimizer, *Ain Shams Eng. J.*, **13** (2022), 101705. https://doi.org/10.1016/J.ASEJ.2022.101705
47. Y. Lu, S. Liang, H. Ouyang, S. Li, G. ge Wang, Hybrid multi-group stochastic cooperative particle swarm optimization algorithm and its application to the photovoltaic parameter identification problem, *Energy Reports*, **9** (2023), 4654–4681. https://doi.org/10.1016/J.EGYR.2023.03.105
48. V. J. Chin, Z. Salam, Coyote optimization algorithm for the parameter extraction of photovoltaic cells, *Sol. Energy*, **194** (2019), 656–670. https://doi.org/10.1016/j.solener.2019.10.093
49. O. S. Elazab, H. M. Hasanien, I. Alsaidan, A. Y. Abdelaziz, S. M. Muyeen, Parameter estimation of three diode photovoltaic model using grasshopper optimization algorithm, *Energies*, **13** (2020), 497. https://doi.org/10.3390/en13020497
50. M. Gafar, S. Sarhan, A. R. Ginidi, A. M. Shaheen, An Improved Bio-Inspired Material Generation Algorithm for Engineering Optimization Problems Including PV Source Penetration in Distribution Systems, *Appl. Sci.*, 15 (2025), 603. https://doi.org/10.3390/APP15020603
51. M. Dehghani, G. Bektemyssova, Z. Montazeri, G. Shaikemelev, O. P. Malik, G. Dhiman, Lyrebird Optimization Algorithm: A New Bio-Inspired Metaheuristic Algorithm for Solving Optimization Problems, *Biomimetics*, **8** (2023), 507. https://doi.org/10.3390/biomimetics8060507
52. A. Khaled, M. Gafar, S. Sarhan, A. M. Shaheen, A. S. Alwakeel, A lyrebird optimizer with mimicry and territory protection mechanisms for spectrum sharing MIMO system with intelligent reflecting surface, *Results Eng.*, **26** (2025), 105519. https://doi.org/10.1016/J.RINENG.2025.105519

53. S. H. Hakmi, H. Alnami, G. Moustafa, A. R. Ginidi, A. M. Shaheen, Modified Rime-Ice Growth Optimizer with Polynomial Differential Learning Operator for Single- and Double-Diode PV Parameter Estimation Problem, *Electronics*, 13 (2024), 1611. https://doi.org/10.3390/ELECTRONICS13091611
54. M. Kumar, A. Kumar, An efficient parameters extraction technique of photovoltaic models for performance assessment, *Sol. Energy*, **158** (2017), 192–206. https://doi.org/10.1016/j.solener.2017.09.046
55. Z. Meng, Y. Zhao, S. Tang, Y. Sun, An efficient datasheet-based parameters extraction method for two-diode photovoltaic cell and cells model, *Renew. Energy*, **153** (2020), 1174–1182. https://doi.org/10.1016/j.renene.2020.02.084
56. A. A. Elbaset, H. Ali, M. Abd-El Sattar, Novel seven-parameter model for photovoltaic modules, *Sol. Energy Mater. Sol. Cells*, **130** (2014), 442–455. https://doi.org/10.1016/j.solmat.2014.07.016
57. K. Tifidat, N. Maouhoub, An efficient method for predicting PV modules performance based on the two-diode model and adaptable to the single-diode model, *Renew. Energy*, **216** (2023), 119102. https://doi.org/10.1016/j.renene.2023.119102
58. A. Ginidi, S. M. Ghoneim, A. Elsayed, R. El-Sehiemy, A. Shaheen, A. El-Fergany, Gorilla Troops Optimizer for Electrically Based Single and Double-Diode Models of Solar Photovoltaic Systems, *Sustainability*, **13** (2021), 9459. https://doi.org/10.3390/SU13169459
59. M. H. Sulaiman, Z. Mustaffa, M. M. Saari, H. Daniyal, Barnacles Mating Optimizer: A new bio-inspired algorithm for solving engineering optimization problems, *Eng. Appl. Artif. Intell.*, **87** (2020), 103330. https://doi.org/10.1016/j.engappai.2019.103330
60. J. Liang, S. Ge, B. Qu, K. Yu, F. Liu, H. Yang, et al., Classified perturbation mutation based particle swarm optimization algorithm for parameters extraction of photovoltaic models, *Energy Convers. Manag.*, **203** (2019), 112138. https://doi.org/10.1016/j.enconman.2019.112138
61. G. Kanimozhi, Harish Kumar, Modeling of solar cell under different conditions by Ant Lion Optimizer with LambertW function, *Appl. Soft Comput. J.*, **71** (2018), 141–151. https://doi.org/10.1016/j.asoc.2018.06.025
62. K. Yu, B. Qu, C. Yue, S. Ge, X. Chen, J. Liang, A performance-guided JAYA algorithm for parameters identification of photovoltaic cell and module, *Appl. Energy*, **237** (2019), 241–257. https://doi.org/10.1016/j.apenergy.2019.01.008
63. H. Ben Aribia *et al.*, Growth Optimizer for Parameter Identification of Solar Photovoltaic Cells and Modules, *Sustainability*, **15** (2023), 7896. https://doi.org/10.3390/su15107896
64. W. Alsaggaf, M. Gafar, S. Sarhan, A. M. Shaheen, A. R. Ginidi, Chemical-Inspired Material Generation Algorithm (MGA) of Single- and Double-Diode Model Parameter Determination for Multi-Crystalline Silicon Solar Cells, *Appl. Sci.*, **14** (2024), 8549. https://doi.org/10.3390/APP14188549
65. R. M. Rizk-Allah, A. A. El-Fergany, Conscious neighborhood scheme-based Laplacian barnacles mating algorithm for parameters optimization of photovoltaic single- and double-diode models, *Energy Convers. Manag.*, **226** (2020), 113522. https://doi.org/10.1016/j.enconman.2020.113522
66. A. F. Nematollahi, A. Rahiminejad, B. Vahidi, A novel physical based meta-heuristic optimization method known as Lightning Attachment Procedure Optimization, *Appl. Soft Comput. J.*, **59** (2017), 596–621. https://doi.org/10.1016/j.asoc.2017.06.033

67. S. M. Ebrahimi, E. Salahshour, M. Malekzadeh, Francisco Gordillo, Parameters identification of PV solar cells and modules using flexible particle swarm optimization algorithm, *Energy*, **179** (2019), 358–372. https://doi.org/10.1016/j.energy.2019.04.218
68. E. E. Ali, M. A. El-Hameed, A. A. El-Fergany, M. M. El-Arini, Parameter extraction of photovoltaic generating units using multi-verse optimizer, *Sustain. Energy Technol. Assessments*, **17** (2016), 68–76. https://doi.org/10.1016/j.seta.2016.08.004
69. F. A. Şenel, F. Gökçe, A. S. Yüksel, T. Yiğit, A novel hybrid PSO–GWO algorithm for optimization problems, *Eng. Comput.*, **35** (2019), 1359–1373. https://doi.org/10.1007/s00366-018-0668-5
70. A. M. Beigi, A. Maroosi, Parameter identification for solar cells and module using a Hybrid Firefly and Pattern Search Algorithms, *Sol. Energy*, **171** (2018), 435–446. https://doi.org/10.1016/j.solener.2018.06.092
71. V. Khanna, B. K. Das, D. Bisht, Vandana, P. K. Singh, A three diode model for industrial solar cells and estimation of solar cell parameters using PSO algorithm, *Renew. Energy*, **78** (2015), 105–113. https://doi.org/10.1016/J.RENENE.2014.12.072
72. G. Moustafa, I. H. Smaili, D. R. Almalawi, A. R. Ginidi, A. M. Shaheen, M. Elshahed, et al., Dwarf Mongoose Optimizer for Optimal Modeling of Solar PV Systems and Parameter Extraction, *Electron.*, **12** (2023), 4990. https://doi.org/10.3390/electronics12244990
73. D. Oliva, E. Cuevas, G. Pajares, Parameter identification of solar cells using artificial bee colony optimization, *Energy*, **72** (2014), 93–102. https://doi.org/10.1016/j.energy.2014.05.011
74. J. J. Liang, A. K. Qin, P. N. Suganthan, S. Baskar, Comprehensive learning particle swarm optimizer for global optimization of multimodal functions, *IEEE Trans. Evol. Comput.*, **10** (2006), 281–295. https://doi.org/10.1109/TEVC.2005.857610
75. X. Chen, K. Yu, W. Du, W. Zhao, G. Liu, Parameters identification of solar cell models using generalized oppositional teaching learning based optimization, *Energy*, 99 (2016), 170–180. https://doi.org/10.1016/j.energy.2016.01.052
76. L. Guo, Z. Meng, Y. Sun, L. Wang, Parameter identification and sensitivity analysis of solar cell models with cat swarm optimization algorithm, *Energy Convers. Manag.*, **108** (2016), 520–528. https://doi.org/10.1016/j.enconman.2015.11.041
77. R. V. Rao, V. J. Savsani, D. P. Vakharia, Teaching-Learning-Based Optimization: An optimization method for continuous non-linear large scale problems, *Inf. Sci.*, **183** (2012), 1–15. https://doi.org/10.1016/j.ins.2011.08.006
78. X. Chen, B. Xu, C. Mei, Y. Ding, K. Li, Teaching–learning–based artificial bee colony for solar photovoltaic parameter estimation, *Appl. Energy*, **212** (2018), 1578–1588. https://doi.org/10.1016/j.apenergy.2017.12.115
79. G. Moustafa, H. Alnami, A. R. Ginidi, A. M. Shaheen, An improved Kepler optimization algorithm for module parameter identification supporting PV power estimation, *Heliyon*, **10** (2024), e39902. https://doi.org/10.1016/J.HELIYON.2024.E39902
80. S. Xu, Y. Wang, Parameter estimation of photovoltaic modules using a hybrid flower pollination algorithm, *Energy Convers. Manag.*, **144** (2017), 53–68. https://doi.org/10.1016/J.ENCONMAN.2017.04.042
81. S. A. Mohamed, A. M. Shaheen, M. H. Alqahtani, B. M. Al Faiya, Enhancement of rime algorithm using quadratic interpolation learning for parameters identification of photovoltaic models, *Sci. Rep.*, **15** (2025), 1–24. https://doi.org/10.1038/s41598-025-04589-x

82. G. Moustafa, H. Alnami, S. H. Hakmi, A. Ginidi, A. M. Shaheen, F. A. Al-Mufadi, An Advanced Bio-Inspired Mantis Search Algorithm for Characterization of PV Panel and Global Optimization of Its Model Parameters, *Biomimetics*, **8** (2023), 490. https://doi.org/10.3390/BIOMIMETICS8060490
83. I. Choulli, M. Elyaqouti, E. H. Arjdal, D. Saadaoui, D. Ben hmamou, S. Lidaighbi, et al., An Analytical-Iterative Method for Accurate Parameter Estimation of the Single-Diode Model in Photovoltaic Modules: Application to Monocrystalline and Polycrystalline Modules under Various Environmental Conditions, *Green Energy Intell. Transp.*, **5** (2025) 100285. https://doi.org/10.1016/J.GEITS.2025.100285

AIMS Press